# Influence of extended dwell time during pre- and main compression on the properties of ibuprofen tablets

E. Peeters[a], A.F.T. Silva[b,1], M. Fonteyne[b], T. De Beer[b], C. Vervaet[a], J.P. Remon[a]

[a] Ghent University, Faculty of Pharmaceutical Sciences, Campus Heymans, Laboratory of Pharmaceutical Technology, Ottergemsesteenweg 460, 9000 Ghent, Belgium.

[b] Ghent University, Faculty of Pharmaceutical Sciences, Campus Heymans, Laboratory of Pharmaceutical Process Analytical Technology, Ottergemsesteenweg 460, 9000 Ghent, Belgium.

[1] IAQV/REQUIMTE, Department of Chemical Sciences, Faculty of Pharmacy, University of Porto, Rua Jorge Viterbo Ferreira, 228, 4050-313 Porto, Portugal.

E. Peeters: Elisabeth Peeters, PhD student. Elisabeth.Peeters@Pfizer.com

A.F.T. Silva: Ana Filipa Tavares da Silva, PhD student, Ana.TavaresdaSilva@UGent.be

M. Fonteyne: Margot Fonteyne, PhD student, Thomas.DeBeer@UGent.be

T. De Beer: Thomas De Beer, Professor, Thomas.DeBeer@UGent.be

C. Vervaet: Chris Vervaet, Professor, Chris.Vervaet@UGent.be

J.P. Remon: Jean-Paul Remon, Professor, JeanPaul.Remon@UGent.be

**Corresponding Author**

Chris Vervaet

Ghent University - Faculty of Pharmaceutical Sciences

Campus Heymans

Laboratory of Pharmaceutical Technology

Ottergemsesteenweg 460

9000 Ghent

Belgium

Tel: 0032 9 264 80 69

Fax: 0032 9 222 82 36

E-mail: Chris.Vervaet@UGent.be

**Abstract**

The low melting point, poor flow, physico-mechanical properties (particle size distribution, shape, particle surface roughness) and deformation mechanism of ibuprofen in combination with its high dose in tablets all contribute to the problems observed during the compaction of ibuprofen-based formulations. Since ibuprofen is plastically and elastically deforming, the rate of compaction plays an important role in both the final tablet properties and the risk of capping, laminating and sticking to the punches. While the compaction rate in most tableting machines is only determined by the tableting speed, the high speed rotary tableting machine used in this research project (MODUL$^{TM}$ P, GEA Process Engineering, Halle, Belgium) can adjust and control the dwell time independently from the tableting speed, using an air compensator which allows displacement of the upper (pre-) compression roller. The effect of this machine design on process parameters and tablet properties was investigated. Granules containing 80% ibuprofen were compressed into tablets at 250, 500 and 1000 tablets per minute via double compression (pre- and main compression) with or without extended dwell time. Prior to tableting, granule properties were determined. Process parameters and tablet properties were analyzed using Multivariate Data Analysis. Principal Component Analysis provided an overview of the main phenomena determining the tableting process and Partial Least Squares Analysis unveiled the main variables contributing to the observed differences in the tablet properties.

**Keywords**

Tableting, Rotary tablet press, Displacement, Force-Time profile, Extended dwell time, Multivariate data analysis.

62 **Graphical Abstract**

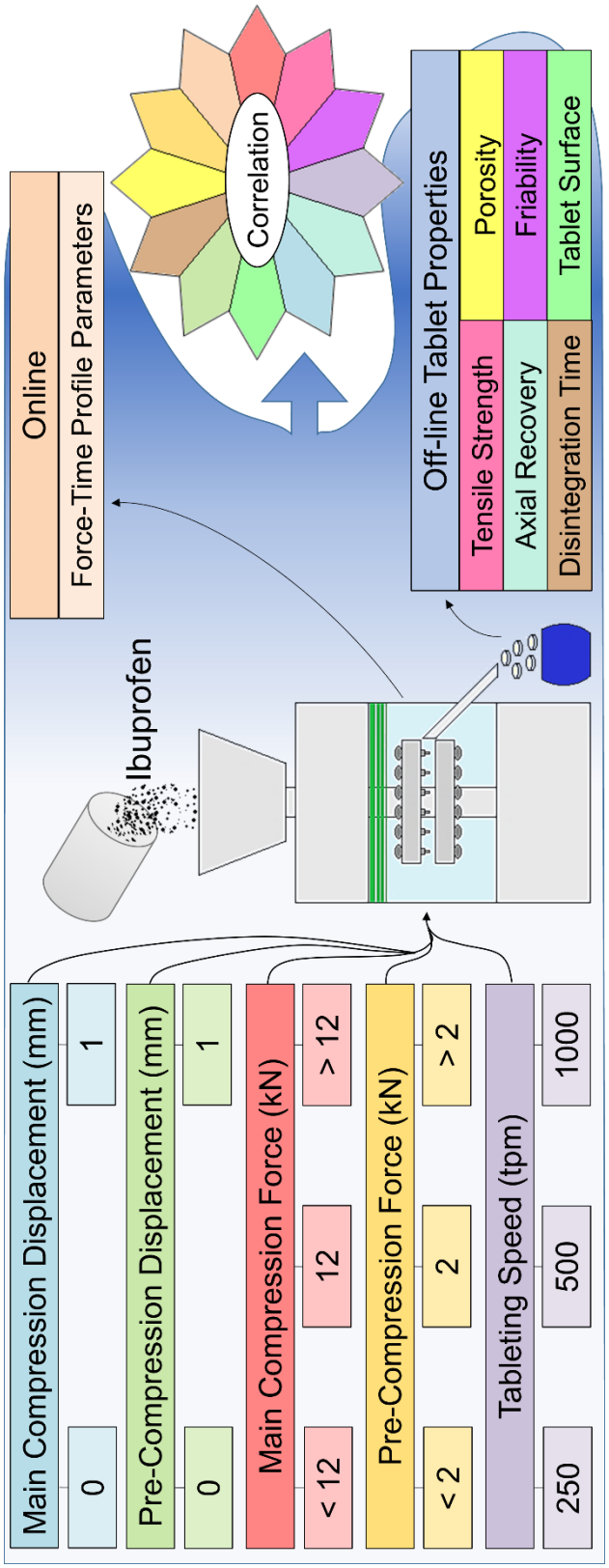

## 1. Introduction

Ibuprofen is widely used for the treatment of rheumatoid arthritis, osteoarthritis and mild and moderate pain, in daily doses ranging from 0.2 to 2.4 g [1]. For high-dosed tablets, the physico-mechanical properties of the pure component play a major role in the tableting process [2, 3]. As a result, the processing of ibuprofen into tablets still encounters problems due to its low melting point, poor flow and deformation mechanism [3-5]. Various attempts were made to improve the tableting behavior of ibuprofen formulations (flowability, tabletability, compactibility) by recrystallization, dry granulation (roller compaction, pressure swing granulation) or dry coating [3-11]. Although these methods contribute to the understanding of the tableting behavior of ibuprofen, the applicability in production settings is limited, due to the rather moderate improvements and long processing times of some methods.

Since the common crystal form (needle-like shape) of ibuprofen undergoes plastic and elastic deformation, the rate of compaction plays an important role in both the final tablet properties and the risk of capping, laminating and sticking to the punches [2, 12, 13]. Besides the compaction rate, also the punch tip geometry, embossment [14] and roughness, as well as the composition of the punch tip coating (i.e. boron-alloy, chrome, …) [15] have an influence on the sticking tendency. Consequently, in industrial manufacturing the production process is optimized either by optimizing the tooling, or reducing the rate of compaction, or both [2, 12-15].

In most tableting machines, the compaction rate (i.e. consolidation phase, dwell time, decompression phase) can only be adjusted by changing the tableting speed [16]. However, using the MODUL$^{TM}$ P high-speed rotary tablet press (GEA Process Engineering, Halle, Belgium) the dwell time can be adjusted and controlled independently of the tableting speed, due to an air compensator which allows displacement of the upper (pre-) compression roll. This design, which has not yet been thoroughly described in literature, could affect the

processability of materials exhibiting a rate-dependent compression behavior, like ibuprofen [2, 12, 13, 17].

The aim of this study was to get a thorough understanding of this compression method (i.e. speed-independent extended dwell time). Using a commercial ibuprofen formulation, the influence of extended dwell time independent of compression speed on the dependent machine parameters and on the tablet properties was examined. Due to the large amount of data obtained (process parameters and tablet characteristics), multivariate data analysis was used to analyze and present results in a structured manner.

## 2. Materials and methods

### 2.1. Materials

Granules, containing 80 % ibuprofen, were kindly donated by Sanico (Turnhout, Belgium), and used as received. The granules were produced by fluid bed wet granulation. A premixed blend of the active pharmaceutical ingredient (API) and a binder were agglomerated with water as the granulation liquid. After drying, a glidant, lubricant and anti-adhesive were added externally.

### 2.2. Granule characterization

Particle size analysis was done by sieve analysis ($n$ = 3), using a sieve shaker (Retsch VE 1000, Haan, Germany). 200 g of granules was placed on a nest of sieves (50, 100, 150, 250, 300, 500, 710, 1000 and 1120 µm) and shaken at an amplitude of 2 mm for 10 min. The amount of granules retained on each sieve was determined. The density ($\rho_{true}$) of the granules was measured ($n$ = 3) using a helium pycnometer (Accupyc 1330 pycnometer, Micrometrics Instruments, Norcross, Georgia, USA), with ten purges and ten runs per measurement. The

bulk ($\rho_{bulk}$) and tapped density ($\rho_{tapped}$) of 30 g of granules was determined in a 100 ml graduated cylinder ($n$ = 3). The powder was poured from a height of 40 cm through a stainless steel funnel with a 10 mm orifice into the graduated cylinder, mounted on a tapping device (J. Engelsmann, Ludwigshafen am Rhein, Germany). Bulk and tapped densities were calculated as 30 g/$V_0$ and 30 g/$V_{1250}$, respectively. These values were used to calculate the compressibility index (CI) in order to assess the tendency of a powder to consolidate [18].

### 2.3. Preparation of tablets

#### 2.3.1. Mechanism of compression

All tablets were prepared by double compression (i.e. a pre-compression and main compression step). At the pre-compression station the punches apply an initial force on the powder, and subsequently, under the main compression rollers the final compression takes place, usually at a higher load compared to the pre-compression phase [19-21]. The role of the pre-compression step is to reduce air-entrapment during the main compression step. Also the extent of stress-relaxation is increased by effectively extending the dwell time via pre-compression, yielding stronger tablets [20-23].

Most rotary tablet presses operate by maintaining fixed roller positions during compression. The upper roller remains in a fixed position, which determines the penetration depth of the upper punch and consequently the in-die tableting position. By adjusting the position of the lower roller, the compression force is determined and hence, the thickness of the compact under compression. Furthermore, for a given tablet press and tooling, the kinetics of the punch movement depend only on the tableting speed. As a result the total contact time (the period when the upper punch is in contact with the powder), the consolidation time (the period during which the punches approach each other), the dwell time (the period during which the punch head flat is in direct contact with the compression roller), the decompression phase (the time

during which the punches move away from each other) and the lag-time (the time between pre-compression and main compression phase) are defined by the tangential velocity of the punch [16, 20-22, 24-37].

In contrast, using the MODUL$^{TM}$ P high-speed rotary tablet press these parameters can be controlled independently from the tableting speed, due to an air compensator which allows displacement of the upper compression rollers (Figure 1). The upper rollers are attached to an air piston, which allows vertical movement in an air cylinder. During a compression run the air pressure in the cylinder ($CF_r$) is set at a constant value due to a control system of pressure valves and expansion vessels. The piston, and consequently the upper roller, is pushed downwards by the air pressure against a fixed stop, being the bottom of the air cylinder. The adjustable position of the lower roller is controlled similar to a conventional tablet press with fixed rollers. During compression, the upper punch initially moves downwards into the die when in contact with the upper roller. As the lower punch is pushed upwards by the lower roller, the powder bed in the die consolidates and the compression force increases. When the reaction force exerted by the powder on the upper punch exceeds the force exerted by the counter pressure (i.e. the air pressure on the piston), upward movement of the upper compression roller is possible. The complete assembly of bottom punch, powder slug and top punch moves simultaneously, following the lower compression roller and consequently raises the upper roller. The distance by which the upper roller is displaced only depends on the position of the lower compression roller. The dwell time is now not only defined by the punch head flat, the pitch diameter and the turret speed, but also by the displacement. As the upper roller is displaced, the contact time between the punch head flat and the roller is prolonged. Hence the dwell time is extended in comparison to the fixed roller set-up, although tableting speed is constant. If, however, a higher air pressure than the force exerted by the powder is set in the cylinder of the air compensator, the upper roller does not move, and the system behaves as a set-up with fixed rollers [17].

This system with moving rollers has major implications on the control systems and kinetics of punch movement, compared to a system with fixed rollers. The shape of the force-time profiles, and mainly the dwell time, is affected, as further discussed in more detail [17, 19, 28, 32]. Another implication of this concept is the effect on the in-die tableting position since the lower roller will have a higher position in order to induce displacement. Therefore, the position of the powder slug in the die will be higher compared to a system with fixed rollers. Hence the distance travelled by the tablet before being ejected is less which can influence the stress applied on the powder bed, resulting in a different relaxation behaviour [22]. A schematic overview of the different positions and movements of rollers and punches is provided in Figure 2.

It is necessary to mention that the term 'displacement' in this research is strictly used to describe *the movement of the upper roller*, and *not* the movement of the punches, as it is done in all previous research describing force-time profiles.

### 2.3.2. Collection of data

The tablet press is equipped with strain gauge-based load cells which are used for force measurement at pre- and main compression and at ejection. Load cells below the lower compression rollers and the ejection cam measure the compression force (CF) and ejection force (EF), respectively. Displacement of pre- and main compression rollers is measured by linear variable displacement transducers (LVDT sensors), which are connected to the upper compression rollers. Punch stroke movement is monitored by LVDT sensors, which are placed inside the turret and are fixed to one keyed punch set by means of clamps.

Collection and analysis of the data was performed with a data acquisition and analysis system (CDAAS) (GEA Process Engineering, Halle, Belgium). The CDAAS software is an application which measures and samples the signals (pre-compression force (PCF), main compression

force (MCF), pre-compression displacement (PCD), main compression displacement (MCD), ejection force (EF) and punch strokes) at high frequency (up to 100 kHz) with 16bit A/D conversion. It allows calibration, filtering, visualization and recording of the processed sensor signals and reviewing and analyzing of recorded data.

### 2.3.3. Tabletability

In order to determine the MCF at which the experiments should be performed, a preliminary tabletability study was performed. Tabletability may be defined as the capacity of a powder to be transformed into a tablet of specified strength under the effect of compaction pressure. It can be represented by a plot of tensile strength (TS) versus compaction pressure [30, 35, 38-41]. Although very useful, the obtained correlation is not an intrinsic material characteristics and the profile is dependent upon the press, tooling and settings used (e.g. tableting speed, paddle speed in the forced feeder, fill depth) [30, 31, 35, 40]. Therefore, the same tooling ($n$ = 10, standard euro B, diameter 12 mm, concave radius 24 mm) was used throughout the study. The fill depth was adjusted to obtain tablets of 500 mg, in accordance with the dwell time experiments. Tableting speed was set at 500 tablets per minute (tpm) and force feeder speeds were kept constant at 25 and 40 rpm. PCF was set at 2 kN and PCD at 0.2 mm. MCD was kept at 0.0 mm for all experiments and MCF was varied from 3 to 30 kN with increments of 3 kN. An extra point at 42 kN MCF was added to examine the TS at a very high compression load. For each experiment the machine was run for 2 minutes, with sampling during the second minute. Room temperature (21.0 ± 2.0 °C) and relative humidity (RH) (30.0 ± 2.0 %) were controlled.

### 2.3.4. Influence of extended dwell time

A series of experiments was conducted in order to investigate the effect of the extended dwell time induced by displacement. Experiments were repeated at three different tableting speeds

231 to examine the effect of this parameter. Initially, the experimental set-up consisted of 12
232 experiments, in which three factors were varied (Table 1). PCF was kept constant at 2 kN and
233 MCF was set at 12 kN, based on the results of the preliminary tabletability test. However, the
234 shape of the force-time signal for tablets compressed with moving rollers induced some set-
235 up modifications, as this profile deviated from the theoretical profile (Figure 3) [35]. This
236 atypical shape is caused by the inertia of the system and is inherently correlated to the design
237 of the air compensator. A limited "overshoot" occurs before the plateau of the extended dwell
238 is reached. Furthermore, the ratio between $F_{top}$ and $F_{mplateau}$ (defined as the mean value of
239 $F_{25dw}$, $F_{50dw}$ and $F_{75dw}$ (see further)) increases at higher tableting speed, which is by default due
240 to the larger impact at higher punch velocities when the punches come into contact with the
241 compression rollers. As a result, two compression forces ($F_{top}$ and $F_{mplateau}$) were taken into
242 account for analysis and correlation with the tablet properties. Hence, PCF and MCF values
243 of 2 kN and 12 kN, respectively, were maintained, in order to be able to compare the
244 experiments between different tableting speeds. Moreover, depending on the tableting speed,
245 the other compression force (with displacement) was determined as the resulting $F_{top}$ by
246 keeping the $F_{mplateau}$ on these preset values (i.e. experiment 3 in Figure 4). This ultimately
247 resulted in an adjusted set-up with seven experiments per tableting speed (total of 20
248 experiments, experiment 12 was not performed), from which a schematic overview is provided
249 in Figure 4. The red bars indicate the set PCF and MCF of 2 and 12 kN respectively. However,
250 when this bar is not located at the top of the curve ($F_{top}$), this indicates that the powder bed is
251 actually exposed to a higher compression force during compression.
252
253 Tablets were prepared on the MODUL$^{TM}$ P, equipped with an overfill cam of 16 mm and using
254 a set of punches as described earlier. The fill depth was adjusted prior to each experiment to
255 obtain tablets of 500 mg. Tableting speed was set at 250, 500 or 1000 tpm, depending on the
256 experiment. As paddle speed must be adjusted in function of tableting speed in order to avoid
257 speed-induced weight variability [42], force feeder speeds were set either at 10 rpm – 50 rpm,
258 25 rpm – 40 rpm or 35 rpm – 50 rpm. PCF, PCD, MCF and MCD were set according to the

experiment (Figure 4). In order to avoid confounding factors, each experiment was run on an empty and cleaned tablet press. The machine was run for 2 minutes, with sampling during the second minute. Room temperature (21.0 ± 2.0 °C) and relative humidity (30.0 ± 2.0 %) were controlled. A summary of the machine settings is given in Table 2.

## 2.4. Data analysis

### 2.4.1. Analysis of process parameters

The CDAAS software stores the collected data from the seven signals as a continuous recording, with time (msec) on the X-axis. PCF, MCF and EF are plotted on one Y-axis (kN), whereas PCD, MCD, movement of bottom punch and movement of upper punch are plotted against distance (mm) (Figure 5).

Force-time profiles are already thoroughly addressed by other authors [16, 32-34, 36, 37]. Although these researchers provided insight and proposed applicable evaluation methods for force-time profiles on rotary tablet presses, all these studies were conducted with a fixed roller set-up. Consequently, the moving roller assembly used in this research and the resulting atypical force-time profile requires a modified analysis protocol. Moreover, since it is possible to compress tablets with both methods (fixed and moving rollers), parameters allowing quantitative comparison between both types of profiles had to be defined. A schematic overview of these parameters is given in Figure 6, which represents a force-time profile without and with displacement (i.e. fixed and moving rollers). Since the shape of the force-time profile without displacement was slightly different for main compression compared to pre-compression, a representation of both (Figure 6a and 6b) is provided. The force-time profiles with displacement were comparable for both stations (Figure 6c).

First, the contact time ($t_{total}$, from $t_{begin}$ to $t_{end}$) and the area under the curve of the complete profile ($AUC_{total}$) were defined as parameters [16, 33, 34]. Subsequently, the force-time profile was divided into three phases: the consolidation phase, the dwell time and the decompression phase [16, 33, 34, 36]. The method used to define these phases on the force-time curves depended if the run was performed with fixed or moving rollers. Using moving rollers, the onset and end of the displacement-time signal clearly marked the beginning and end point of the dwell time. This also allowed easy tracking of the consolidation and decompression phase. In runs with fixed rollers, there is no signal indicating when the punches are vertically aligned with the center of the pressure role. For each tableting speed (250, 500 and 1000 tpm) five consecutive force-time signals of the first run (experiment 1 in Figure 4, pre- and main compression without displacement) were aligned on the X-axis by means of an algorithm with five consecutive force-time signals of the second run (experiment 2 in Figure 4, pre- and main compression with displacement). As the middle of the displacement-time signal of experiment 2 marks the center of the compression role, by default it also marks the middle of the dwell time on the force-time profile for both aligned experiments. Knowledge about the middle of the dwell time ($t_{50dw}$) allows correct positioning of the dwell time on the force-time profile. The dwell time ($t_{dw}$) (msec) itself, for the force-time signals without displacement, was calculated according to Equation (1) [43]:

$$t_{dw} = \frac{6\times10^4\times R_h}{\pi\times\omega\times R_p} \qquad (1)$$

Where $R_h$, $R_p$ and $\omega$ denote the radius of the punch head flat (mm), half of the pitch circle diameter of the turret (mm) and the turret speed (rpm), respectively.

In order to allow a faster determination of $t_{50dw}$ for the other experiments without displacement, an empirical method was derived. For main compression, the dwell time of the force-time profiles without displacement were characterized by the same force at the beginning of the

dwell time ($F_{bdw}$) as at the end ($F_{edw}$) (Figure 6a). Therefore, the onset and end of the dwell time were defined by the intersections between the force-time profile and a horizontal line with a length equal to the theoretical calculated dwell time. For pre-compression, the endpoint of the dwell time on the force-time profile without displacement was characterized by a rather sudden and sharp drop in the force profile ($F_{edw}$) (Figure 6b). Consequently, the onset of the dwell time was determined based on this sharp decrease of the force using a line parallel to the X-axis with a length equal to the theoretical dwell time.

Next to the dwell time ($t_{dw}$), the middle of the dwell time ($t_{50dw}$) and the forces at the beginning and the end of the dwell time ($F_{bdw}$ and $F_{edw}$ respectively), additional parameters for this phase were determined. The force at 25% ($F_{25dw}$), 50% ($F_{50dw}$) and 75% ($F_{75dw}$) of the dwell time and the respectively absolute time-points ($t_{25dw}$, $t_{50dw}$, $t_{75dw}$) were determined. The same procedure was followed for the maximum and minimum force occurring during the dwell time ($F_{max}$, $t_{Fmax}$; $F_{min}$, $t_{Fmin}$). The maximum force is also referred to as $F_{curve}$ or $F_{top}$ (Figure 3), depending on compression without or with displacement, respectively. $F_{mplateau}$ was determined as the mean value of $F_{25dw}$, $F_{50dw}$ and $F_{75dw}$. Furthermore, a dimensionless parameter describing the shape of the force-time profile, independent of the absolute force values used, was included: the $t/p_{mean}$ ratio was defined as the ratio between $F_{max}$ and $F_{mplateau}$.

For the consolidation phase, the consolidation time ($t_{con}$, from $t_{begin}$ to $t_{bdw}$), the area under the cuve ($AUC_{con}$) and the slope ($S_{con}$) were defined as parameters. The decompression phase was analyzed accordingly ($t_{decomp}$, from $t_{edw}$ to $t_{end}$; $AUC_{decomp}$; $S_{decomp}$) [16, 24, 33, 34]. As observed in Figure 6, both the consolidation and the decompression phases make up a small portion of the entire profile when displacement is used, characterized by a shorter time span and a steeper slope.

From the ejection profile (yellow line on Figure 5) only the maximum ejection force ($F_{ejec}$) was considered.

As stated above, the displacement-time profiles (red and orange line on Figure 5) were used to measure the dwell time on the force-time profiles. Furthermore, the maximum displacement (CD) was taken into account for further analysis. The signals for bottom punch and top punch movement (blue and purple line on Figure 5) were used to calculate the in-die thickness of the powder plug. The minimum in-die thickness ($T_{ID}$) was calculated by determining the minimum distance between the bottom and upper punch during compression ($h_{BT}$), for both pre- and main compression. Furthermore, the distance between the punches immediately after pre- and main compression ($T_{AD}$) was measured in order to calculate the in-die immediate axial recovery (IAR) of the material after each compression step. The point at which the measurement was performed was determined by simultaneously taking into account the punch stroke profile (movement of the punches) and the force-time profile of the same punch. This point was determined as the point immediately after the force dropped to zero and the punches stopped following the movement of the compression rollers. Finally, based on the movement of the bottom punch, the time between the end of punch movement at pre-compression and the beginning of punch movement at main compression was defined as the lag-time ($t_{lag}$) [20, 21].

For each run, consecutive force-time ($n$ = 10), displacement-time ($n$ = 10) and punch motion ($n$ = 3) signals were analyzed. Data were then exported for further statistical pretreatment and computations prior to PCA analysis. A schematic overview of all parameters is given in Table 3.

### 2.4.2. Tablet evaluation

An overview of the examined tablet characteristics is provided in Table 4. In order to obtain information about the influence of the tableting parameters on the granules both “in-die” as well as “out-of-die”, tablet evaluation was done immediately after production (t0) and after a

storage period of seven days (t7). Friability, disintegration and SEM were only performed after the storage period. Tablets were stored in open tablet trays in a sealed container at 23.1 ± 1.0 °C and 30.0 ± 2.0 % relative humidity (using a saturated solution of magnesium chloride hexahydrate (Fagron, Waregem, Belgium)).

Tablets (*n* = 10) were weighed and their hardness, thickness and diameter was determined (Sotax HT 10, Basel, Switserland). The tablet tensile strength (*TS*) was calculated using Equation (2) [44].

$$TS = \frac{2F}{\pi dt} \qquad (2)$$

Where *F, d* and *t* denote the diametral crushing force (N), the tablet diameter (mm) and the tablet thickness (mm), respectively.

Tablet friability was determined on 13 tablets using a friabilator described in the European Pharmacopeia (Pharma Test PTF-E, Hainburg, Germany), at a speed of 25 rpm for 4 min. Tablets were dedusted and weighed prior to and after the test. Tablet friability was expressed as the percentage weight loss. The disintegration time of the tablets (*n* = 9) was evaluated with the Pharma Test PTZ-E (Hainburg, Germany) as described in the European Pharmacopoeia. Tests were performed in distilled water at 37.0 ± 0.5 °C using disks. The disintegration time was determined as the time when no visible particles remained on the mesh wire.

In order to calculate the porosity (ε) of the tablets, the apparent density ($\rho_{app}$) of the tablets was determined. For the in-die density determination, tablet volume was calculated using Equation (3), according to the diameter of the die, dimensions of the punch tip and the in-die thickness ($T_{ID}$), derived from the distance between the top and bottom punch ($h_{BT}$). For out-of-

die determination four dimensions of 10 tablets with known weight were measured with a projection microscope (Reickert, 96/0226, Vienna, Austrich). Subsequently, the volume of the tablet was calculated according to Equation (3), with *D* (mm)*, H* (mm)*, h* (mm) and *R* (mm) the diameter, the total height determined in the middle, the height of the central cylinder and the radius of the concave part of the tablet, respectively. Weight divided by the volume of the tablet resulted in the apparent density ($\rho_{app}$). Based on the true density of the granules ($\rho_{true}$) determined by helium pycnometry, the porosity of the tablets was calculated according to Equation (4).

$$V = \left[\pi \times \left(\frac{D}{2}\right)^2 \times h\right] + 2 \times \left[\frac{1}{3} \times \pi \times \left(\frac{H-h}{2}\right)^2 \times \left[3 \times R - \left(\frac{H-h}{2}\right)\right]\right] \qquad (3)$$

$$\varepsilon = \left(1 - \frac{\rho_{app}}{\rho_{true}}\right) \times 100 \qquad (4)$$

Several definitions are used to characterize immediate axial tablet expansion or recovery (*IAR*) (%) [25, 40, 41, 45]. In general, IAR describes the difference between the minimum tablet thickness under maximum compression force ($T_{ID}$) (mm) and the tablet thickness after the pressure is removed ($T_A$) (mm), as represented by Equation (5) [45].

$$IAR = \left(\frac{T_A - T_{ID}}{T_{ID}}\right) \times 100 \qquad (5)$$

However, there is a discrepancy between the interpretations of different authors about that latter data point. Some authors define the tablet height at the end of the decompression phase, before the tablet is ejected from the die ($T_{AD}$) [25, 41, 46]. Others measure the tablet thickness immediately after ejection from the die ($T_{t0}$) [40, 47] or even after a defined period (e.g. 1 minute) after ejection ($T_{tx}$) [45, 47]. Since each of these different determinations contributes to the understanding of the behavior of the granules in the compression cycle, both definitions

(before and after ejection) were used in this research. Consequently, three different values of IAR were obtained:

- $IAR_{pre}$: the immediate axial recovery after pre-compression, with $T_A$ and $T_{ID}$ the tablet thickness measured in-die immediately after the decompression phase ($T_{AD}$) and the minimum tablet thickness under maximum pre-compression force, respectively.
- $IAR_{main}$: similar to $IAR_{pre}$, but calculated for the main compression phase.
- $IAR_{t0}$: the axial relaxation of the tablet after ejection, where $T_A$ denotes the tablet height immediately after ejection ($T_{t0}$) and $T_{ID}$ the tablet height under maximum compression force at main compression ($T_{IDM}$).

Furthermore, after a recovery period of seven days, the cumulative axial recovery (CAR) was calculated accordingly (Equation (6)) [45]:

$$CAR = \left(\frac{T_{t7} - T_{IDM}}{T_{IDM}}\right) \times 100 \qquad (6)$$

With *CAR* the cumulative axial recovery (%), $T_{t7}$ the tablet height after a storage period of seven days (mm) and $T_{IDM}$ the tablet height under maximum compression force at main compression (mm), respectively. Additionally, the hardening of the tablets (%) upon storage was calculated using Equation (7):

$$Hardening = \left(\frac{TS_{t7} - TS_{t0}}{TS_{t0}}\right) \times 100 \qquad (7)$$

With $TS_{t0}$ and $TS_{t7}$ the tablet tensile strengths (MPa) measured immediately after ejection from the die and after seven days of storage, respectively. In order to simplify the evaluation of the influence of the storage period on the tablet characteristics, a few additional parameters were defined. Diff(CAR-IAR), Diff W, Diff T, Diff D, Diff H and Diff TS represent the changes in axial

relaxation, weight, thickness, diameter, hardness and tensile strength of the tablets during storage, respectively.

SEM was used to study the tablet surface. The tablets were mounted on metal stubs with carbon tape and further processed as described for the granule characterization. The tablets were observed at magnifications of 1000x and 2000x.

### 2.4.3. Multivariate data analysis

All calculated mean values and variation coefficients of the machine settings, the data logged by the tablet press and the CDAAS software and the tablet properties were combined in a data table (20 rows, 169 columns) [48]. Principal Component Analysis (PCA) was performed on the machine settings and logged data obtained from the tableting press and CDAAS (*X*, Tables 2 and 3) in order to provide an overview of the performed experiments and investigate the correlations between all process variables. A Partial Least Squares (PLS) regression model was developed to explore the correlations between the machine settings and logged data (*X*) and the tablet properties (*Y*, Table 4). Variables were scaled to unit variance prior to analysis [49]. The multivariate model was developed with the Simca P+ 13 software (Umetrics AB, Umeå, Sweden).

## 3. Results and discussion

### 3.1. Granule characteristics

An overview of the flow properties, true density and particle size distribution of the granules is presented in Table 5. Scanning electron microscope (SEM) pictures (not shown) taken from the material showed that the ibuprofen crystals are needle-like shaped. This observation, in combination with the large fraction of smaller particles detected in the mixture, contributed to

the classification of this powder as a fairly flowing powder based on the compressibility index values.

### 3.2. Tabletability

The influence of MCF on TS is depicted in Figure 7. The TS increases with MCF at compression pressures less than 18 kN. Above 18 kN, the curve gradually levels off to a plateau, where a further increase in the compaction force does not contribute to a higher tensile strength. The higher energy put in the system is not used for additional bond formation and can, in some cases, even decrease the strength of formed bonds, as elastic expansion at higher compression forces is favored [2, 12, 13, 38]. The preferred compression force from a manufacturing point of view is the lowest force (i.e. the least energy input) at which tablets complying with quality- and bioavailability requirements can be produced. The variability in TS however, is significantly larger when a variation (e.g. 0.5 kN) in MCF occurs at lower compression forces, due to the higher slope of the curve at lower compression forces (under 10 kN). Since this could be a confounding factor, commonly a force closer to the plateau of the curve is chosen. Consequently, 12 kN was chosen as MCF for further experiments. At this CF, TS still depends on CF and the influence of variation in CF stays rather limited.

### 3.3. Multivariate Data Analysis

#### 3.3.1. Principal Component Analysis

Four principal components (PCs) were fitted in the PCA model explaining 81.9% ($R^2$) of the variation in the data. The first, second, third, and fourth PC explained 29.0%, 24.9%, 19.1%, and 9.8%, respectively.

Figure 8 depicts the scores of PC1 versus the scores of PC2. Three obvious clusters on the X-axis (PC1) are identifiable: experiments on the left side were performed at a speed of 250tpm, on the center at a speed of 500tpm and on the right at a speed of 1000tpm. PC1, the first PC in the model, is found by searching in the multivariate space for the direction of the largest variance. This elucidates again how important the tableting speed is in performing tableting experiments, as it contributes the most to the observed variance. To investigate in detail how the tableting speed is related to the other process parameters, a loading plot is constructed (Figure 9). Scores and loadings have a strong association, and both plots should be observed simultaneously. Observations in a particular place on the score plot have high values for the variables in the same place in the loading plot (positively correlated) and low values for the variables at the opposite site of the loading plot (negatively correlated). Moreover, the effect is more pronounced further away from the origin (i.e. from the middle) of the plot [49]. On the right side of the loading plot (Figure 9), four process variables cluster with the tableting speed (red full circle): fill, $S_{con}$ (P), $S_{con}$ (M) and $T_{AD}$ (M). As tableting speed increases, the fill depth (fill) for powders not exhibiting a free-flowing behavior commonly has to be increased to allow sufficient die filling during the short exposure time to the feeder in order to reach the desired weight. The positive correlation between the after-die thickness ($T_{AD}$) and the tableting speed confirms the observations of other researchers, who stated that an increased tableting speed is able to increase the immediate elastic expansion [12, 20, 25, 27, 40, 50]. $S_{con}$ shows that the tableting speed is closely correlated to the shape of the force-time profile, as this value, representing the slope of the consolidation phase, for both pre- (P) and main compression (M) are significantly increased at high speed. This conclusion is further supported by the cluster situated at the left side of the loading plot, where nearly all other speed related variables of the force-time profile (the area under the curve (AUC) and the different time points (t)) are grouped (red dashed circle). These variables have a higher numerical value when the tableting speed is decreased.

When looking at the score of PC1 versus the scores of PC2 (Figure 8) along the Y-axis (PC2), two clusters can be distinguished. Loadings for PC2 (Figure 9) show that experiments with a lower score value (lower half of the score plot) were performed at a higher MCD (at the bottom of the loading plot (blue full line)) while experiments with higher PC2 scores (upper half of the score plot) were performed at a lower MCD, which is in accordance with the set-up of the experiments (see also Figure 4). Moreover, experiments with a high score value according to PC2 have a high loading value for $MCF_r$, Mbot and Mtop as these process parameters can be found at the top of the loading plot, opposite from the MCD (blue dashed circle). This is understandable, as the counterforce in the air compensator ($MCF_r$) has to be lowered and the position of the lower roller has to be raised (Mbot decreased) to allow more upward vertical displacement (MCD) of the compression rollers. Obviously, with displacement, the position of the upper roller will also be raised (Mtop decreased).

Several other variables are positively or negatively correlated to MCD as seen on Figure 9 (blue dotted circles). Firstly, the inverse correlation between MCD and the ejection force ($F_{ejec}$) is an interesting finding worth mentioning. An explanation for this observation can be that with displacement the ejection is facilitated (ejection force lowered), since compression happens higher in the die. Secondly, the model shows the relation between the MCD and the variability of the process. A cluster close to MCD on the loading plot with VC $t_{Fmax}$, VC $t_{dw}$ and VC $T_{IDM}$ highlight that during compression with displacement the variation in dwell time, in the point when maximum force occurs and in in-die thickness is larger than in experiments were no displacement is used. On the opposite site of the loading plot however, a cluster of VC $F_{mplateau}$, VC $F_{max}$ and VC $AUC_{total}$ reveal that the value of these variables is lowered when displacement is used. From these observations can be concluded that during compression with the moving roller set-up, the variability in the process is not translated into variability in the force exerted on the powder bed, as is the case with the fixed roller set-up.

Finally, the parameters positioned in the left lower corner of the loading plot are positively correlated to the MCD. From this can be concluded that during the experiments with displacement the compression event is statistically prolonged, as the total contact time ($t_{total}$), the dwell time ($t_{dw}$) and related values ($AUC_{total}$, $t_{25dwl}$, $t_{50dw}$, $t_{75dw}$, $t_{Fmin}$) are increased. In contrast, $t_{Fmax}$ can be found at the upper part of the loading plot, so negatively correlated with an increased displacement. This observation becomes clear when looking at the difference in shape of the force-time profile with and without displacement (Figure 6a and Figure 6c). For all former parameters ($t_{25dwl}$, $t_{50dw}$, $t_{75dw}$, $t_{Fmin}$) the difference between that data point and the beginning of the dwell time ($t_{bdw}$) becomes larger when using displacement. For the latter ($t_{Fmax}$) exactly the opposite effect can be seen. The fact that these process parameters are located on the loading plot more to the left instead of center bottom, indicates that both the tableting speed (PC1) and the displacement at main compression (PC2) are correlated with these parameters. This means that the influence of MCD will be more elucidated at lower tableting speeds. A similar conclusion can be drawn when looking at the position of $t/p_{mean}$ on the loading plot. As it is located closer to the lower right corner, both a higher tableting speed and a higher displacement contribute to this value. As mentioned previously, the atypical shape of the force-time profile with displacement is caused by the inertia of the system and is inherently correlated to the design of the air compensator. Furthermore, the ratio between $F_{top}$ and $F_{mplateau}$ increases at higher tableting speed, which is by default due to the larger impact at higher punch velocities when the punches come into contact with the compression rolls. From this can be concluded that the $t/p_{mean}$ ratio is a sensitive parameter to describe the shape of the force-time profile within the range of the parameter setting used.

Figure 10 depicts the scores of PC3 versus the scores of PC4 and accordingly, Figure 11 represents the loadings of PC3 versus the loadings of PC4. According to PC3 there are two obvious clusters which by looking at the loadings plots can be attributed to differences in the PCD. Experiments with a lower score value (left side of the score plot) were performed at a higher PCD (left side of the loading plot (blue full line)) while experiments with higher PC3

585 scores (right side of the score plot) were performed at a lower PCD, which is also in
586 accordance with the set-up of the experiments (see also Figure 4). Some of the observed
587 relations show similarity with those observed between the score and loading plot according to
588 PC2. For instance, experiments with a high score value according to PC3 have a high loading
589 value for $PCF_r$, Pbot and Ptop as these process parameters can be found at the complete right
590 side of the loading plot, opposite from the PCD (blue dashed circle). The same rationale as
591 with main compression displacement can be followed to explain these observations.
592 Furthermore, the model shows the relation between the PCD and the variability of the process.
593 A cluster close to PCD on the loading plot with VC $t_{dw}$ and VC $T_{IDP}$ highlight that during
594 compression with displacement the variation in dwell time and in in-die thickness is larger than
595 in experiments were no displacement is used. Also here a cluster of VC $F_{mplateau}$, VC $F_{max}$ and
596 VC $AUC_{total}$ on the opposite site of the loading plot, reveal that the value of these variables is
597 lowered when displacement is used. From these observations can be concluded that also
598 during pre-compression with the moving roller set-up, the variability in the process is not
599 translated into variability in the force exerted on the powder bed, as is the case with the fixed
600 roller set-up.
601
602 Several other variables are positively or negatively correlated to PCD as seen on Figure 11
603 (blue dotted circles). Their position on the loading plot can be explained by the difference in
604 the shape of the force-time profile between compression with and without displacement
605 (Figure 6a and Figure 6c). Firstly, the position of the $t/p_{mean}$ close to the PCD confirms that this
606 value is a suitable parameter to describe the shape of the force-time profile. Furthermore, for
607 the Y-axis of the force-time profile (force), the location of $F_{max}$ and $F_{bdw}$ for pre-compression
608 are logically, as these variables have a higher value when displacement is used. Since $F_{75dw}$,
609 $F_{min}$ and $F_{edw}$ can be found on the opposite site of the plot, these variables are negatively
610 correlated with PCD, $F_{max}$ and $F_{bdw}$. When comparing Figure 6a and Figure 6c, indeed can be
611 seen that these values are lower when displacement is used. $F_{25dw}$ and $F_{50dw}$ are not
612 significantly altered by compressing with or without displacement, which is supported by the

613 position of these variables in the loading plot, since they are located in the middle of the plot
614 according to PC3. For the X-axis of the force-time profile (time), the dwell time ($t_{dw}$) and related
615 values ($t_{25dwl}$, $t_{50dw}$, $t_{75dw}$, $t_{Fmin}$) are increased. In contrast, $t_{decomp}$ can be found at the right side
616 of the loading plot, so is negatively correlated with an increased displacement. From this can
617 be concluded that also during pre-compression the dwell time with the moving-roller is
618 prolonged.
619
620 When looking at the score of PC3 versus the scores of PC4 (Figure 10) along the Y-axis
621 (PC4), two clusters can be distinguished. Loadings for PC4 (Figure 11) show that experiments
622 with a lower score value (lower half of the score plot) were performed at a higher MCF (at the
623 bottom of the loading plot (red full line)) while experiments with higher PC4 scores (upper half
624 of the score plot) were performed at a lower MCF, which is also in accordance with the set-up
625 of the experiments (Figure 4). Closely correlated variables to the MCF ($F_{max}$) are clearly
626 clustered ($F_{bdw}$, $F_{25dw}$, $F_{50dw}$, $F_{75dw}$, $F_{mplateau}$, $F_{edw}$, $F_{min}$), as can be seen on the loading plot.
627 Moreover, experiments with a high score value according to PC4 have a high loading value
628 for $T_{IDM}$ and $h_{BP(M)}$ as these process parameters can be found at the top of the loading plot,
629 opposite from the MCF (red dashed circle). This is expected, as the in-die thickness ($T_{IDM}$) and
630 distance between the punches ($h_{BP}$) is decreased when higher compression forces are used.
631
632 Based on the PCA-analysis, a few general conclusions can be drawn. Firstly, tableting speed
633 contributes to a large extent to the variance of PC1, the first PC in the model. This elucidates
634 how important tableting speed is in performing tableting experiments, as it contributes the
635 most to the observed variance. Mainly its influence on the shape of the force-time profile and
636 the dwell time has to be considered. Secondly, this analysis shows that the moving roller set-
637 up also influences to a great extent the tableting process
638 Moreover, the dimensionless parameter, $t/p_{mean}$ ratio, can be considered a sensitive
639 parameter to describe the shape of the force-time profile within the range of the parameter
640 setting used. Finally, the main compression force contributes to a large extent to the variance

captured by PC4. Since PC4 only explains 9.8 % of the observed variance in the model, it can be concluded that the tableting speed and the displacement have a larger influence on the compression event (i.e. the other process variables) than the applied (main compression) force.

### 3.3.2. Partial Least Squares

In order to examine the influence of the process parameters on the tablet properties, a PLS model was constructed. PLS is a regression extension of PXA, which is used to connect the information in two blocks of variables, *X* (the process parameters) and *Y* (the tablet properties) [49]. In a first attempt to construct the model, all selected variation coefficients (VC) were included in the model (see Table 3 and Table 4). However, a negative $Q^2$ value was obtained for the first 2 PC's. This implies that the model has no predictive power when using only 2 PC's, and a third PC is necessary to force the model into cross validation predictions. Since this approach has no rational basis, the model was adapted and all variation coefficients were excluded. In this new model, three principal components (PCs) were fitted in the PLS model explaining 66.8% ($R^2$) and predicting 18.1% ($Q^2$) of the variation in the data.

Scores of PC1 versus PC2 are depicted in Figure 12. Figure 13 is a plot of the loadings of PC1 versus the loadings of PC2. Again, three clusters on the X-axis (PC1) are identifiable: experiments on the left side were performed at a speed of 1000 tpm, on the center at a speed of 500 tpm and on the right at a speed of 250 tpm. This is confirmed when looking at the loading plot, where the variable speed is positioned on the left side of the plot (red full circle). The loadings of the tablet properties located close to the variable speed are correlated with this process parameter (red dashed circle). Mainly all the "Diff" variables, which depict the difference between the mean value of the process parameter measured at t0 and t7, are related to the tableting speed. Since these variables have a high value, this means that the values of these process parameters are higher after 1 week of storage, than measured

669 immediately after production. The observations can be explained by the viscoelastic behavior
670 of ibuprofen. $IAR_{pre}$ and $IAR_{main}$ have high values at high tableting speed. This means that the
671 immediate axial recovery (in-die) is higher at higher tableting speeds, as also reported in
672 literature [12, 20, 25, 27, 40, 50]. The axial recovery (relaxation) continuous further after
673 removal from the die and during storage (Diff (CAR-IAR)), as an increase in diameter (Diff D)
674 and thickness (Diff T) can be observed. Not only the dimensions of the tablet change, but also
675 an increase in tensile strength takes place, represented by Diff H, Diff TS and Hardening. This
676 suggest that the tablet not only expands slowly due to the viscoelastic nature of the material,
677 but that at the same time a reorganization of the material inside the tablet takes place,
678 contributing to a higher tensile strength. Although already reported in literature, a clear
679 explanation for this effect cannot be given [47]. Moreover, since the absolute values are small
680 (e.g. for thickness a maximum increase of 0.11 mm, diameter 0.03 mm and TS 0.16 MPa) this
681 dos not necessary imply any bio-relevant or critical qualitative changes.
682
683 When looking at the score of PC1 versus the scores of PC2 (Figure 12) along the Y-axis
684 (PC2), no clear clusters can be distinguished. Moreover, based on the experimental settings
685 (Figure 4) and the loadings for PC2 (Figure 13) it is clear that more than one process
686 parameter is contributing to the variance captured by PC2. The loading plot shows that
687 experiments with a lower score value (lower half of the score plot) were performed at a higher
688 MCD and a higher MCF (at the bottom of the loading plot (blue full circle)) while experiments
689 with higher PC2 scores (upper half of the score plot) were performed at a lower MCD and a
690 lower MCF. The loadings of the tablet properties close to these two process variables are the
691 hardness (H), TS and density (dens) of the tablets, both at t0 and t7 (blue dashed circle). The
692 correlation with a higher compression force is obvious, the contribution of the prolonged dwell
693 time (higher MCD) however as such cannot be determined. On the opposite site of the plot,
694 the tablet porosity (t0 and t7) can be found, as this parameter is the inverse of density.
695

Scores of PC2 versus PC3 are depicted in Figure 14. Figure 15 is a plot of the loadings of PC2 versus the loadings of PC3. Although two clusters on the Y-axis (PC3) are identifiable, it is clear that more than one process parameter is contributing to the variance captured by PC3. The loading plot shows that experiments with a higher score value (upper half of the score plot) were performed at a higher MCF and a higher PCF (at the left upper corner and top of the loading plot (blue full circle)) while experiments with lower PC3 scores (lower right corner and bottom of the score plot) were performed at a lower MCF and a lower PCF. The loading of the tablet property close to the process variable PCF is the in- die density (dens ID (P)) (blue dashed circle). On the opposite site of the plot, the in-die porosity (por ID (P)) and in-die volume (V ID (P)) can be found. The loadings of the tablet properties close to the process variable MCF (blue dotted circle) are immediate axial recovery upon ejection (IAR t0) and the axial recovery after storage (CAR). From this can be concluded that when tablets are compressed at higher loads, the relaxation over time is prolonged. Moreover, based on these observations it is clear that different process parameters have a different influence on the relaxation behavior of material (i.e. the correlation between $IAR_{pre}$, $IAR_{main}$ and tableting speed and the correlation between $IAR_{t0}$, CAR with MCF) and that it is important to take all these measurements into consideration. Other tablet properties related to a higher compression force are the density, hardness and TS. On the opposite side of the plot, the porosity, volume and thickness of the tablets are situated. It is interesting to note that the final tablet properties are mainly determined by the final compression (i.e. main compression) step and not so much by the pre-compression step, as the in-die properties at main compression (i.e. dens ID (M), por ID (M), V ID (M) are closely related to the properties after ejection (and after storage) . Since the process variable MCD is also located close to the loadings of the former tablet properties (density, TS, H) it is possible that a higher MCD contributes to these tablet characteristics, although clear conclusions cannot be drawn.

Overall, the PLS revealed that mainly the tableting speed and the main compression force attribute to the final tablet properties. Furthermore, the relation between process parameters

and tablet properties is not straight forward, as the different variables all contribute simultaneously to the final tablet characteristic and the variation captured by the different PC's cannot be linked to one particular process variable. Although displacement seems to contribute to (some of) the tablet characteristics, clear conclusions cannot be drawn. Finally, a special reference should be made to the elastic behavior of ibuprofen. The PLS revealed that a high compression speed and a high MCF both favor the elastic expansion (either in-die or after ejection). This effect is known to increase the capping tendency of tablets. Although not translated in the absolute values of hardness or friability, it should be mentioned that the detrimental effect of higher elastic recovery at high speeds and high compression forces was observed during friability and hardness testing. A large amount of tablets from experiment 3 and 5 at 1000 tpm (Figure 4) underwent capping upon radial pressure before breaking at the hardness test after the storage period (33 and 50 % respectively). Also, during the friability test, about half of these tablets broke into smaller pieces.

### 3.4. Disintegration testing and SEM

The data obtained from the disintegration test were not included in the PLS-analysis, as the observed differences were not bio-relevant, with the shortest disintegration time being 102.57 ± 26.09 s and the longest 167.95 ± 18.06 s. A trend could be observed however, depending on tableting speed and applied forces. The tableting speed had a negative influence on the disintegration time, whereas an increase of the compression force increased the time the tablets needed to disintegrate.

SEM-pictures were taken from the tablet surfaces (not shown). Overall, it could be concluded that the surfaces of the tablets were similar, although an influence of the tableting speed and the compression force could also here be observed. In those experiments where lower tableting speeds and higher compression forces were used, a slightly smoother surface was obtained. The difference becomes more pronounced when comparing the experiments (of

each tableting speed) who were performed with and without displacement (extended dwell time), and this both on pre- and main compression. The tablets produced with displacement had markedly smoother surfaces than the tablets produced without. This observation might explain partly the lower ejection forces obtained with displacement at main compression, as could be concluded from the PCA-analysis. Smoother surfaces will adhere less to the punch tips and die-wall, reducing the force necessary to overcome this adherence and consequently lowering the ejection force.

## 4. Conclusions

Principal Component Analysis (PCA) provided an overview of the main underlying phenomena in the performed tableting experiments. The main source of variation in this dataset was captured in PC1 which is composed mainly by the changes caused by an alteration of the tableting speed. The second major direction of variation in the dataset (PC2) is the change in main compression displacement. PC3 is mainly composed by the displacement at pre-compression and correlated variables. At last, the main compression force contributes to a large extent to the variance captured by PC4. Partial Least Squares (PLS) revealed that mainly the tableting speed and the main compression force attribute to the final tablet properties and that the relation between process parameters and tablet properties is not straight forward, as the different variables all contribute simultaneously to the final tablet characteristics. Overall, this analysis provided a summary of the contribution of the moving roller set-up to the tableting process and tablet properties. This research project shows that a large amount of parameters influence the compression cycle and it is difficult, if not impossible, to study the contribution of all factors separately. Using an instrumented high speed rotary press, a large amount of information is obtained which contributes to the further understanding of this complex engineering process.

## Acknowledgements

Authors would like to thank Sanico (Turnhout, Belgium) for their kind donation of the granules. Dr. Ir. Frederik Detobel and Benny Van der Steen from GEA Process Engineering (Halle, Belgium) are gratefully acknowledged for the fruitful discussions and their technical support in this work.

## Data Statement

Primary raw data could not be provided as they are only available in a format readable by the customized software application (CDAAS). The data table (20 rows, 169 columns) which was used for the multivariate data analysis was made electronically available. It contains all calculated mean values and variation coefficients of the machine settings, the data logged by the tablet press and the CDAAS software and the tablet properties [48].

## Declarations of Interest

None.

## References

[1] C. De Brabander, C. Vervaet, L. Van Bortel, J.P. Remon, Bioavailability of ibuprofen from hot-melt extruded mini-matrices, Int. J. Pharm. 271 (2004) 77-84. doi: 10.1016/j.ijpharm.2003.10.029

[2] P.V. Marshall, P. York, J.Q. Maclaine, An investigation of the effect of the punch velocity on the compaction properties of ibuprofen, Powder Technol. 73 (1993) 171-177. doi: 10.1016/0032-5910(93)87009-D

[3] N. Rasenack, B.W. Müller, Crystal habit and tableting behavior, Int. J. Pharm. 244 (2002) 45-57. doi: 10.1016/S0378-5173(02)00296-X

[4] N.F. Abu Bakar, A. Mujumdar, S. Urabe, K. Takano, K. Nishii, M. Horio, Improvement of sticking tendency of granules during tabletting process by pressure swing granulation, Powder Technol. 176 (2007) 137-147. doi: 10.1016/j.powtec.2007.02.037

[5] K. Kachrimanis, G. Kistis, S. Malamataris, Crystallisation conditions and physicomechanical properties of ibuprofen-Eudragit® S100 spherical crystal agglomerates prepared by the solvent-change technique, Int. J. Pharm. 173 (1998) 61-74. doi: 10.1016/S0378-5173(98)00191-4

[6] P. Di Martino, M. Beccerica, E. Joiris, G.F. Palmieri, A. Gayot, S. Martelli, Influence of chystal habit on the compression and densification mechanism of ibuprofen, J. Cryst. Growth 243 (2002) 345-355. doi: 10.1016/S0022-0248(02)01523-3

[7] H.A. Garekani, D. Sadeghi, A. Badiee, S.A. Mostafa, A.R. Rajabi-Siahboomi, Crystal habit modifications of ibuprofen and their physicomechanical characteristics, Drug Dev. Ind. Pharm. 27 (2001) 803-809. doi: 10.1081/DDC-100107243

[8] P.K. More, K.S. Khomane, A.K. Bansal, Flow and compaction behaviour of ultrafine coated ibuprofen, Int. J. Pharm. 441 (2013) 527-534. doi: 10.1016/j.ijpharm.2012.10.048

[9] S. Patel, A.M. Kaushal, A.K. Bansal, Compaction behavior of roller compacted ibuprofen, Eur. J. Pharm. Biopharm. 69 (2008) 743-749. doi: 10.1016/j.ejpb.2008.01.005

[10] N. Rasenack, B.W. Müller, Ibuprofen crystal with optimized properties, Int. J. Pharm. 245 (2002) 9-24. doi: 10.1016/S0378-5173(02)00294-6

[11] L. Seton, M. Roberts, F. Ur-Rehman, Compaction of recrystallised ibuprofen, Chem. Eng. J. 164 (2010) 449-452. doi: 10.1016/j.cej.2009.10.037

[12] A. Nokhodchi, M.H. Rubinstein, H. Larhrib, J.C. Guyot, The effect of moisture on the properties of ibuprofen tablets, Int. J. Pharm. 118 (1995) 191-197. doi: 10.1016/0378-5173(94)00354-8

[13] A. Nokhodchi, M.H. Rubinstein, H. Larhrib, J.C. Guyot, The effect of moisture content on the energies involved in the compaction of ibuprofen, Int. J. Pharm. 120 (1995) 13-20. doi: 10.1016/0378-5173(94)00372-C

[14] M. Roberts, J.L. Ford, G.S. MacLeod, J.T. Fell, G.W. Smith, P.H. Rowe, Effects of surface roughness and chrome plating of punch tips on the sticking tendencies of model ibuprofen formulations, J. Pharm. Pharmacol. 55 (2003) 1223-1228. doi: 10.1211/0022357021684

838 [15] M. Roberts, J.L. Ford, G.S. MacLeod, J.T. Fell, G.W. Smith, P.H. Rowe, A.M. Dyas,
839 Effects of punch tip geometry and embossment on the punch tip adherence of a model
840 ibuprofen formulation, J. Pharm. Pharmacol. 56 (2004) 947-950. doi: 10.1211/0022357023736

841 [16] M. Leitritz, M. Krumme, P.C. Schmidt, Force-time curves of a rotary tablet press.
842 Interpretation of the compressibility of a modified starch containing various amounts of
843 moisture, J. Pharm. Pharmacol. 48 (1996) 456-462. doi: 10.1111/j.2042-7158.1996.tb05954.x

844 [17] J. Van Evelghem, Improving tablet quality with compression to equal force technology,
845 Pharm. Tech. (Suppl.) 32 (2008) 26-29.

846 [18] R.L. Carr, Evaluating flow properties of solids, Chem. Eng. 72 (1965) 163-168.

847 [19] M. J. Bogda, Tablet compression: Machine theory, design, and process troubleshooting,
848 in: J. Swarbrick (Ed.), Encyclopedia of pharmaceutical technology Informa Healthcare USA
849 Inc., New York, 2007, pp.3611-3629.

850 [20] O. F. Akande, J.L. Ford, P.H. Rowe, M.H. Rubinstein, The effects of lag-time and dwell-
851 time on the compaction properties of 1:1 paracetamol/microcrystalline cellulose tablets
852 prepared by pre-compression and main compression, J. Pharm. Pharmacol. 50 (1998) 19-28.
853 doi: 10.1111/j.2042-7158.1998.tb03300.x

854 [21] C.E. Ruegger, M. Celik, The influence of varying precompaction and main compaction
855 profile parameters on the mechanical stenth of compacts, Pharm. Dev. Technol. 5 (2000) 495-
856 505. doi: 10.1081/PDT-100102033

857 [22] I.C. Sinka, F. Motazedian, A.C.F. Cocks, K.G. Pitt, The effect of processing parameters
858 on pharmaceutical tablet properties, Powder Technol. 189 (2009) 276-284. doi:
859 10.1016/j.powtec.2008.04.020

860 [23] E.N. Hiestand, J.E. Wells, C.B. Peot, J.E. Ochs, Physical processes in tableting, J. Pharm.
861 Sci. 66 (1977) 510-519. doi: 10.1002/jps.2600660413

862 [24] N.A. Armstrong, Tablet manufacture, in: J. Swarbrick (Ed.), Encyclopedia of
863 pharmaceutical technology Informa Healthcare USA Inc., New York, 2007, pp.3653-3672.

864 [25] R.V. Haware, I. Tho, A. Bauer-Brandl, Evaluation of a rapid approximation method for the
865 elastic recovery of tablets, Powder Technol. 202 (2010) 71-77. doi:
866 10.1016/j.powtec.2010.04.012

867 [26] T.M. Jones, The physicochemical properties of starting materials used in tablet
868 formulation, Int. J. Pharm. Tech. Prod. Manuf. 2 (1981) 17-24.

869 [27] P. Konkel, J.B. Mielck, Associations of parameters characterizing the time course of the
870 tabletting process on a reciprocating and on a rotary tabletting machine for high-speed
871 production, Eur. J. Pharm. Sci. 45 (1998) 137-148. doi: 10.1016/S0939-6411(98)00020-4

872 [28] M. Levin, Tablet press instrumentation, in: J. Swarbrick (Ed.), Encyclopedia of
873 pharmaceutical technology Informa Healthcare USA Inc., New York, 2007, pp.3684-3706.

874 [29] A. Munoz Ruiz, M.R. Jimenez-Castellanos, J.C. Cunningham, A.V. Katdare, Theoretical
875 estimation of dwell and consolidation times in rotary tablet machines, Drug Dev. Ind. Pharm.
876 18 (1992) 2011-2028. doi: 10.3109/03639049209040917

877 [30] A.S. Narang, V.M. Rao, H. Guo, J.A. Lu, D.S. Desai, Effect of force feeder on tablet
878 strength during compression, Int. J. Pharm. 401 (2010) 7-15. doi:
879 10.1016/j.ijpharm.2010.08.027

880 [31] C.E. Ruegger, M. Celik, The effect of compression and decompression speed on the
881 mechanical strength of compacts, Pharm. Dev. Technol. 5 (2000) 485-494. doi: 10.1081/PDT-
882 100102032

883 [32] C.E. Rowlings, A.Y. Leung, P.C. Sheen, Resolution of the material and machine
884 contributions to the area to height ratio obtained from force-time powder compression data II:
885 Rotary tablet press, Pharm. Acta Helv. 72 (1997) 125-130. doi: 10.1016/S0031-
886 6865(97)00008-3

887 [33] P.C. Schmidt, P.J. Vogel, Force-time-curves of a modern rotary tablet machine I.
888 Evaluation techniques and characterization of deformation behaviour of pharmaceutical
889 substances, Drug Dev. Ind. Pharm. 20 (1994) 921-934. doi: 10.3109/03639049409038341

890 [34] P.C. Schmidt, M. Leitritz, Compression force/time-profiles of microcrystalline cellulose,
891 dicalcium phosphate dihydrate and their binary mixtures – a critical consideration of
892 experimental parameters, Eur. J. Pharm. Biopharm. 44 (1997) 303-313. doi: 10.1016/S0939-
893 6411(97)00129-X

894 [35] C.K. Tye, C. Sun, G.E. Amidon, Evaluation of the effects of tableting speed on the
895 relationships between compaction pressure, tablet tensile strength, and tablet solid fraction,
896 J. Pharm. Sci. 94 (2005) 465-472. doi: 10.1002/jps.20262

[36] P.J. Vogel, P.C. Schmidt, Force-time curves of a modern rotary tablet machine II. Influence of compression force and tableting speed on the deformation mechanisms of pharmaceutical substances, Drug Dev. Ind. Pharm. 19 (1993) 1917-1930. doi: 10.3109/03639049309073898

[37] J.K. Yliruusi, O.K. Antikainen, New parameters derived from tablet compression curves. Part I. Force-Time curve, Drug Dev. Ind. Pharm. 23 (1997) 69-79. doi: 10.3109/03639049709148483

[38] C. Sun, D.J.W. Grant, Influence of crystal structure on the tableting properties of sulfamerazine polymorphs, Pharm. Res. 18 (2001) 274-280. doi: 10.1023/A:1011038526805

[39] C. Sun, M.W. Himmelspach, Reduced tabletability of roller compacted granules as a result of granule size enlargement, J. Pharm. Sci. 95 (2006) 200-206. doi: 10.1002/jps.20531

[40] S.L. Cantor, S.W. Hoag, L.L. Augsburger, Evaluation of the mechanical properties of extrusion-spheronized beads and multiparticulate systems, Drug Dev. Ind. Pharm. 35 (2009) 683-693. doi: 10.1080/03639040802526797

[41] E. Joiris, P. Di Martino, C. Berneron, A.M. Guyot-Hermann, J.C. Guyot, Compression behavior of orthorhombic paracetamol, Pharm. Res. 15 (1998) 1122-1130. doi: 10.1023/A:1011954800246

[42] E. Peeters, T. De Beer, C. Vervaet, J.P. Remon, Reduction of tablet weight variability by optimizing paddle speed in the forced feeder of a high-speed rotary tablet press, Drug Dev. Ind. Pharm. 41 (2015) 530-539. doi: 10.3109/03639045.2014.884121

[43] D. Natoli, M. Levin, L. Tsygan, L. Liu, Development, optimization, and scale-up of process parameters: Tablet compression, in: Y. Qiu, Y. Chen, G.G.Z. Zhang, L. Liu, W.R. Porter (Eds.), Developing Solid Oral Dosage Forms, Pharmaceutical Theory and Practice, Elsevier Inc., New York, 2009, pp. 725-759.

[44] J.T. Fell, J.M. Newton, Determination of Tablet Strength by Diametral-Compression Test, J. Pharm. Sci. 59 (1970) 688-691. doi: 10.1002/jps.2600590523

[45] N.A. Armstrong, R.F. Haines-Nutt, Elastic recovery and surface area changes in compacted powder systems, J. Pharm. Pharmacol. 24 (1972) 135P-136P. doi: 10.1016/0032-5910(74)80054-9

926 [46] A. Adolfsson, C. Nystrom, Tablet strength, porosity, elasticity and solid state structure of
927 tablets compressed at high loads, Int. J. Pharm. 132 (1996) 95-106. doi: 10.1016/0378-
928 5173(95)04336-5

929 [47] K.M. Picker, Time dependence of elastic recovery for characterization of tableting
930 materials, Pharm. Dev. Technol. 6 (2001) 61-70. doi: 10.1081/PDT-100000014

931 [dataset] [48] E. Peeters, A.F.T. Silva, M. Fonteyne, T. De Beer, C. Vervaet, J.P. Remon, Data
932 Table of Influence of extended dwell time during pre- and main compression on the properties
933 of ibuprofen, Mendeley Data, v1, 2018. http://dx.doi.org/10.17632/drwddcpyn7.1

934 [49] L. Eriksson, E. Johansson, N. Kettaneh-Wold, J. Trygg, C. Wikström, S. Wold, Multi- and
935 Megavariate data analysis, part I, basic principles and applications, second ed., Umetrics,
936 Umea, 2006.

937 [50] R.J. Roberts, R.C. Rowe, The effect of punch velocity on the compaction of a variety of
938 materials, J. Pharm. Pharmacol. 37 (1985) 377-384. doi: 10.1111/j.2042-7158.1985.tb03019.x

## Tables

Table 1: Initial set-up of the experimental design.

Table 2: Overview of the machine settings. The settings included in the PCA and PLS-analysis are marked with ◆.

Table 3: Overview of parameters derived from the logged data. The settings included in the PCA and PLS-analysis are marked: ◆ if only the absolute value was taken into account, ◆◆ if also the variation coefficient (VC) was included in the data.

Table 4: Overview of the tablet characteristics. The settings included in the PLS-analysis are marked: ◆ if only the absolute value was taken into account, ◆◆ if also the variation coefficient (VC) was included in the data.

Table 5: Flow properties, true density and particle size distribution of the granules.

955 Table 1: Initial set-up of the experimental design.

| Process variable | Lower level | Mid level | Upper level |
|---|---|---|---|
| Tableting speed (tpm) | 250 | 500 | 1000 |
| Precompression displacement (mm) | 0 | - | 1 |
| Main compression displacement (mm) | 0 | - | 1 |

Table 2: Overview of the machine settings. The settings included in the PCA and PLS-analysis are marked with ◆.

| Key | Meaning | Incl. |
|---|---|---|
| speed (tpm) | Tableting speed | ◆ |
| pad1 (rpm) | Speed of paddle 1 in the forced feeder | |
| pad2 (rpm) | Speed of paddle 2 in the forced feeder | |
| fill (mm) | Fill depth, which determines the weight | ◆ |
| $CF_r$ (kN) [a] | Air pressure in the air-compensator above the top roller | ◆ |
| bot (mm) [a] | Position of bottom roller | ◆ |
| top (mm) [a] | Position of top roller | ◆ |

[a] Different values for pre- (P) and main (M) compression.

Table 3: Overview of parameters derived from the logged data. The settings included in the PCA and PLS-analysis are marked: ◆ if only the absolute value was taken into account, ◆◆ if also the variation coefficient (VC) was included in the data.

| Key | Meaning | Incl. |
|---|---|---|
| Force-Time profile [a] | | |
| $AUC_{totlal}$ (kN*ms) | Area under the curve of the complete profile | ◆◆ |
| $t_{total}$ (ms) | Contact time | ◆◆ |
| $AUC_{con}$ (kN*ms) | Area under the curve of the consolidation phase | ◆ |
| $t_{con}$ (ms) | Consolidation time | ◆ |
| $S_{con}$ | Slope of the consolidation phase | ◆ |
| $AUC_{decomp}$ | Area under the curve of the decompression phase | ◆ |
| $t_{decomp}$ (ms) | Decompression time | ◆ |
| $S_{decomp}$ | Slope of the decompression phase | ◆ |
| $t_{dw}$ (ms) | Dwell time | ◆◆ |
| $F_{bdw}$ (kN) | Force at the beginning of the dwell time | ◆ |
| $F_{edw}$ (kN) | Force at the end of the dwell time | ◆ |
| $t_{25dw}$ (ms) | First quarter of the dwell time | ◆ |
| $F_{25dw}$ (kN) | Force at 25% of the dwell time | ◆ |
| $t_{50dw}$ (ms) | Middle of the dwell time | ◆ |
| $F_{50dw}$ (kN) | Force at 50% of the dwell time | ◆ |
| $t_{75dw}$ (ms) | Third quarter of the dwell time | ◆ |
| $F_{75dw}$ (kN) | Force at 75% of the dwell time | ◆ |
| $t_{Fmax}$ (ms) | Time when maximum force occurs | ◆◆ |
| $F_{max}$ (kN) | Maximum force | ◆◆ |
| $t_{Fmin}$ (ms) | Time when minimum force occurs | ◆ |
| $F_{min}$ (kN) | Minimum force | ◆ |
| $F_{mplateau}$ (kN) | Mean force of $F_{25dw}$, $F_{50dw}$, $F_{75dw}$ | ◆◆ |
| $t/p_{mean}$ | Ratio of $F_{max}$ to $F_{mplateau}$ | ◆ |
| Ejection profile | | |
| $F_{ejec}$ (kN) | Maximum ejection force | ◆ |
| Displacement-time profiles [a] | | |
| CD (mm) | Maximum displacement of the upper roller | ◆ |
| Punch strokes | | |
| $h_{BT}$ (mm) [a] | Minimum distance between upper and lower punch during compression | ◆ |
| $T_{ID}$ (mm) [a] | Minimum in-die thickness during compression | ◆◆ |
| $T_{AD}$ (mm) [a] | In-die thickness immediately after the decompression phase | ◆ |
| $t_{lag}$ (ms) | The time between pre- and main compression, measured on lower roller | ◆ |

[a] Different values for pre- (P) and main (M) compression.

963 Table 4: Overview of the tablet characteristics. The settings included in the PLS-analysis are
964 marked: ◆ if only the absolute value was taken into account, ◆◆ if also the variation coefficient
965 (VC) was included in the data.

| Key | Meaning | Incl. |
|---|---|---|
| W (mg) [a] | Tablet weight | ◆ |
| T (mm) [a] | Tablet thickness | ◆◆ |
| D (mm) [a] | Tablet diameter | ◆ |
| H (N) [a] | Hardness | ◆ |
| TS (MPa) [a] | Tensile strength | ◆◆ |
| Fria (%) | Friabiltiy | ◆ |
| Disint (s) | Disintegration | |
| $V_{ID}$ [b] | Volume of the tablets during compressing, with minimum distance between punches | ◆ |
| V [a] | Volume of the tablets after ejection | ◆ |
| $\rho_{ID}$ [b] | Density of the tablets during compressing, with minimum distance between punches | ◆ |
| P [a] | Density of the tablets after ejection | ◆ |
| $\varepsilon_{ID}$ [b] | Porosity of the tablets during compressing, with minimum distance between punches | ◆◆ |
| E [a] | Porosity of the tablets after ejection | ◆◆ |
| $IAR_{pre}$ (%) | Immediate axial recovery after the decompression phase at pre-compression | ◆ |
| $IAR_{main}$ (%) | Immediate axial recovery after the decompression phase at main compression | ◆ |
| $IAR_{t0}$ (%) | Immediate axial recovery of the tablets after ejection from the die | ◆ |
| CAR (%) | Cumulative axial recovery of the tablets after a storage period of 7 days | ◆ |
| Hardening (%) | Change in TS of the tablets upon storage | ◆ |
| Diff (CAR-IAR) | Difference between the $IAR_{t0}$ and CAR | ◆ |
| Diff W (mg) | Difference in weight between t0 and t7 | ◆ |
| Diff T (mm) | Difference in thickness between t0 and t7 | ◆ |
| Diff D (mm) | Difference in diameter between t0 and t7 | ◆ |
| Diff H (N) | Difference in hardness between t0 and t7 | ◆ |
| Diff TS (MPa) | Difference in tensile strength between t0 and t7 | ◆ |

966 [a] Different values for measurements immediately after ejection (t0) and after the storage period
967 (t7).

968 [b] Different values for pre- (P) and main (M) compression.

969 Table 5: Flow properties, true density and particle size distribution of the granules.

| $\rho_{bulk}$(g/cm$^3$) | $\rho_{tapped}$ (g/cm$^3$) | CI (%) | $\rho_{true}$(g/cm$^3$) | Particle size distribution | | |
|---|---|---|---|---|---|---|
| | | | | d10 (µm) | d50 (µm) | d90 (µm) |
| 0.56 ± 0.00 | 0.67 ± 0.01 | 17.34 ± 0.59 | 1.24 ± 0.00 | 11.6 ± 0.6 | 66.2 ± 0.8 | 527.3 ± 3.5 |

970

## Figures

Figure 1: Schematic representation of the pneumatic air compensator.

Figure 2: Schematic overview of the different positions and movements of rollers and punches (a) with fixed rollers and (b) with moving rollers, highlighted by red lines and arrows. −·−· depicts the punch movement of the upper punch, −−− depicts the movement of the lower punch.

Figure 3: Representative illustration of theoretical (I) and observed (II) compression profile for tablets compressed without (a) and with (b) displacement.

Figure 4: Schematic overview of the performed experiments. Red bars indicate the initial force (2 kN at pre-compression, 12 kN at main compression).

Figure 5: Example of the data-logging. X-asis represent time (ms), left Y-axis represent distance (mm), right Y-axis represents force (kN). Offset on Y-axis is intentionally changed to permit better visibility of different values.

Figure 6: Schematic overview of the parameters determined from the force-time profiles for tablets compressed without displacement at main compression (a) and pre-compression (b) and with displacement (c) (both at pre- and main compression).

Figure 7: Plot representing the tabletability. Tensile strength (TS) is plotted against main compression force (MCF).

Figure 8: Score scatter plot of PC1 vs. PC 2. [t1] Scores of Principal Component 1; [t2] Scores of Principal Component 2.

Figure 9: Loading scatter plot of PC1 vs. PC 2. [p1] Scores of Principal Component 1; [p2] Scores of Principal Component 2. Key: see Table 2 and Table 3.

Figure 10: Score scatter plot of PC3 vs. PC 4. [t3] Scores of Principal Component 3; [t4] Scores of Principal Component 4.

Figure 11: Loading scatter plot of PC3 vs. PC 4. [p3] Loadings of Principal Component 3; [p4] Loadings of Principal Component 4. Key: see Table 2 and Table 3.

Figure 12: Score scatter plot of PC1 vs. PC 2. [t1] Scores of Principal Component 1; [t2] Scores of Principal Component 2.

Figure 13: Loading scatter plot of PC1 vs. PC 2. w*c[1] Loadings of Principal Component 1; w*c[2] Loadings of Principal Component 2. Key: see Table 2, Table 3 and Table 4.

Figure 14: Score scatter plot of PC2 vs. PC 3. [t2] Scores of Principal Component 2; [t3] Scores of Principal Component 3.

Figure 15: Loading scatter plot of PC2 vs. PC 3. w*c[2] Loadings of Principal Component 2; w*c[3] Loadings of Principal Component 3. Key: see Table 2, Table 3 and Table 4.

Figure 1: Schematic representation of the pneumatic air compensator.

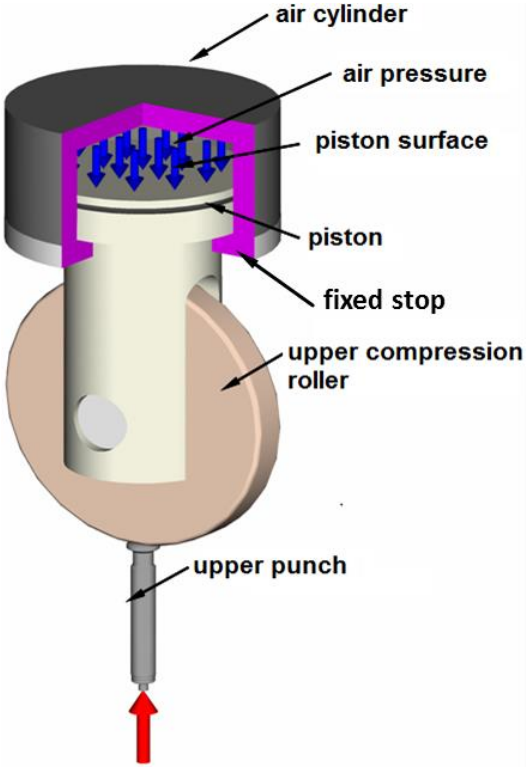

Figure 2: Schematic overview of the different positions and movements of rollers and punches (a) with fixed rollers and (b) with moving rollers, highlighted by red lines and arrows. −·−· depicts the punch movement of the upper punch, −−− depicts the movement of the lower punch.

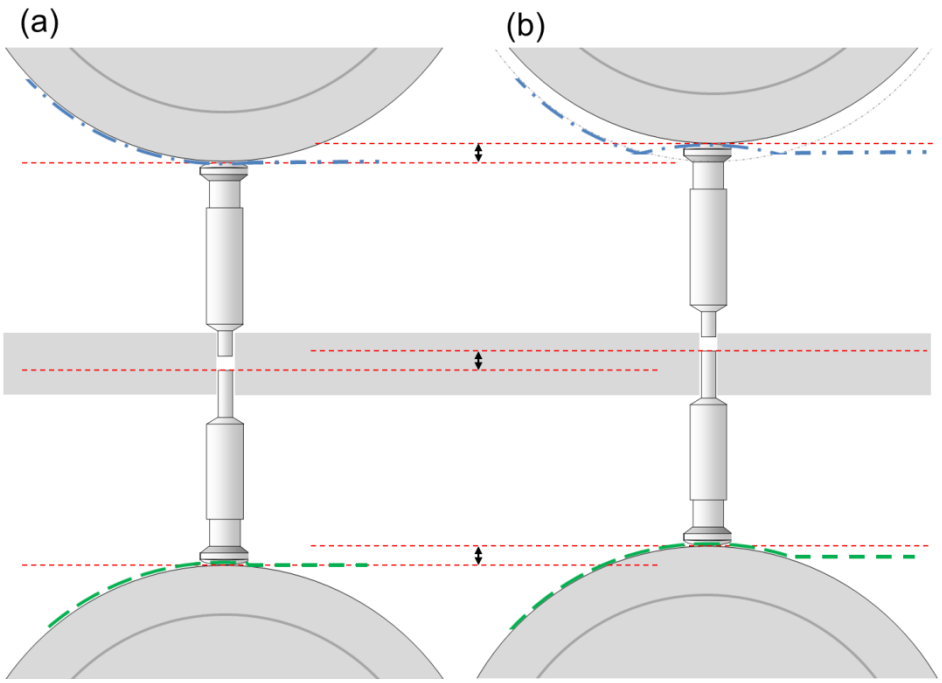

Figure 3: Representative illustration of theoretical (I) and observed (II) compression profile for tablets compressed without (a) and with (b) displacement.

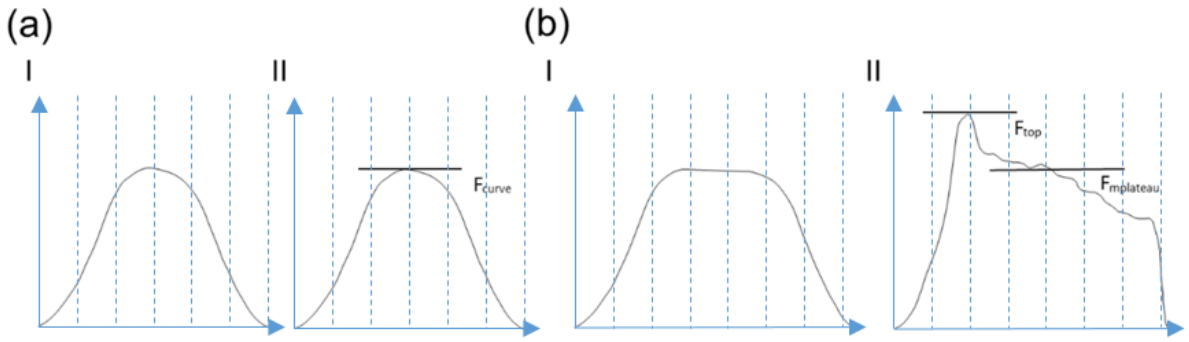

Figure 4: Schematic overview of the performed experiments. Red bars indicate the initial force (2 kN at pre-compression, 12 kN at main compression).

| Speed (tpm) 250 | 500 | 1000 Experiment | Precompression Shape | Precompression Displacement | Main compression Shape | Main compression Displacement |
|---|---|---|---|---|---|---|
| 1 | 8 | 15 | 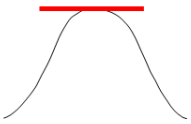 | no | 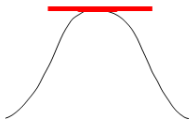 | no |
| 2 | 9 | 16 | 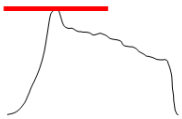 | yes | 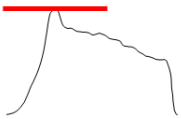 | yes |
| 3 | 10 | 17 | 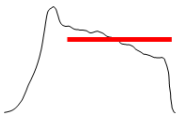 | yes | 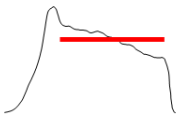 | yes |
| 4 | 11 | 18 | 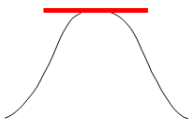 | no | 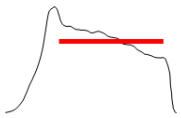 | yes |
| 5 | 12 | 19 | 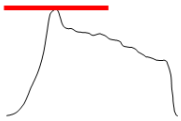 | yes | 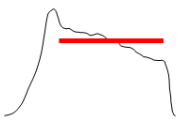 | yes |
| 6 | 13 | 20 | 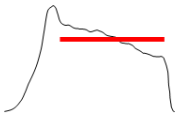 | yes | 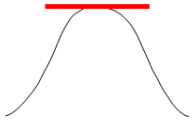 | no |
| 7 | 14 | 21 | 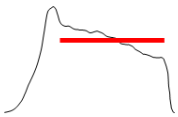 | yes | 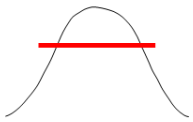 | no |

Figure 5: Example of the data-logging. X-asis represent time (ms), left Y-axis represent distance (mm), right Y-axis represents force (kN). Offset on Y-axis is intentionally changed to permit better visibility of different values.

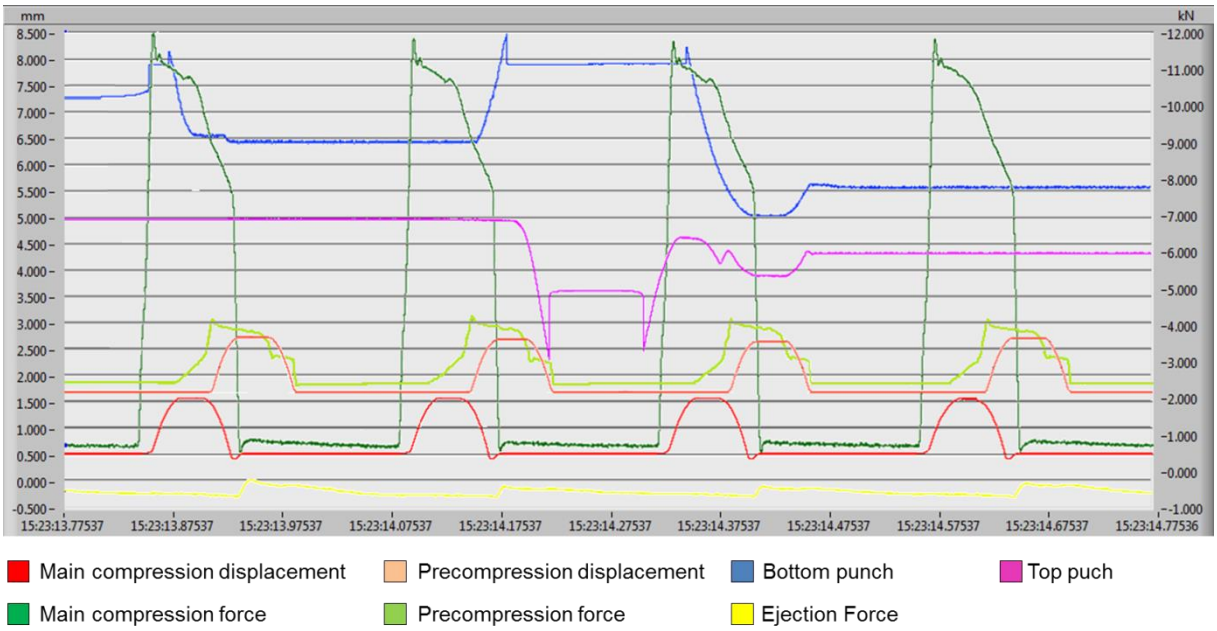

Figure 6: Schematic overview of the parameters determined from the force-time profiles for tablets compressed without displacement at main compression (a) and pre-compression (b) and with displacement (c) (both at pre- and main compression).

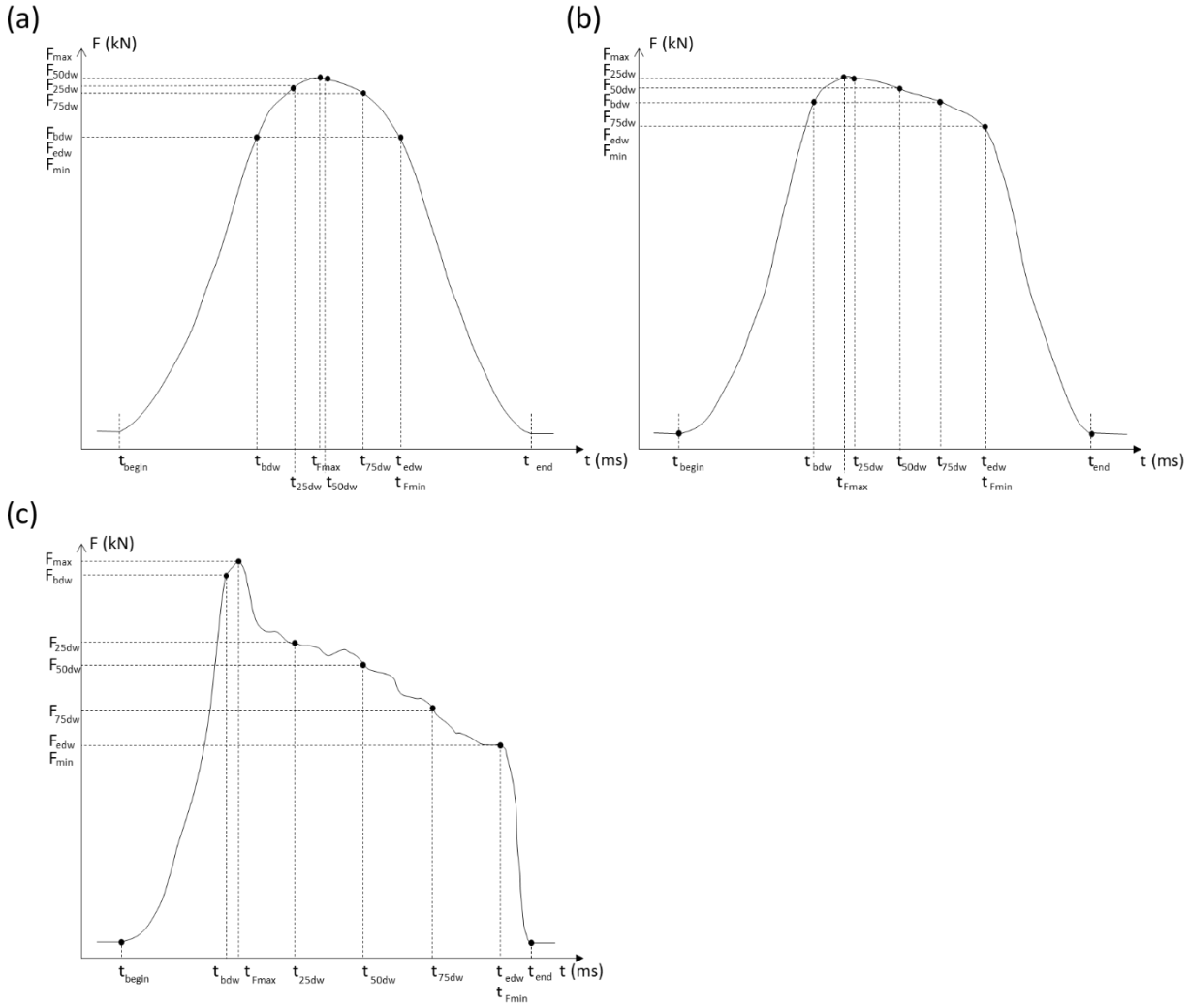

1035 Figure 7: Plot representing the tabletability. Tensile strength (TS) is plotted against main

1036 compression force (MCF).

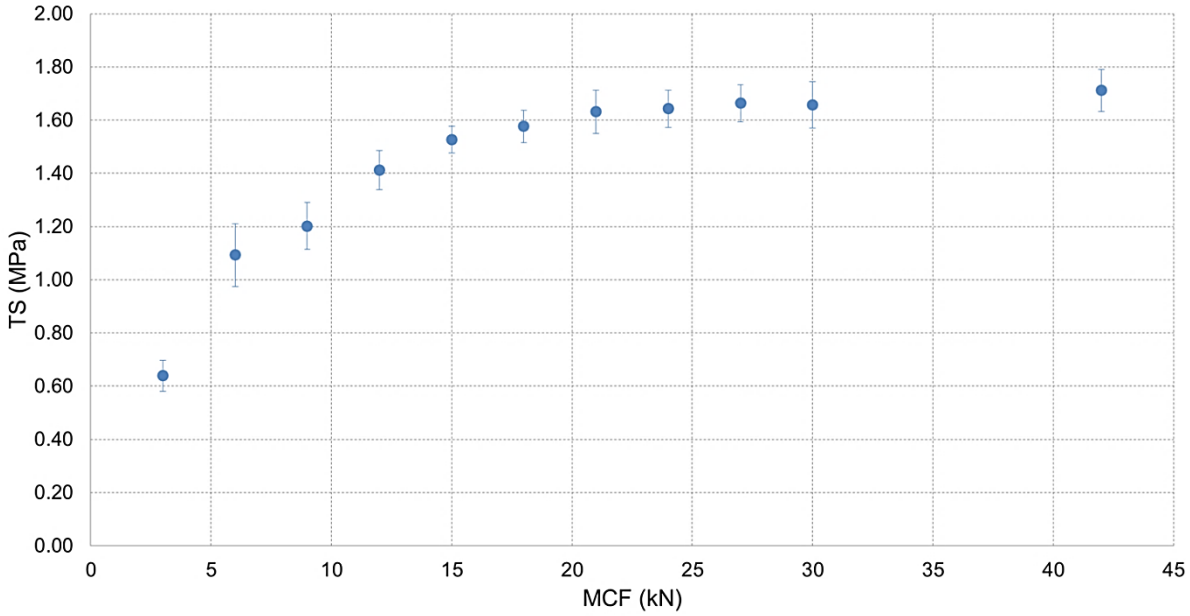

Figure 8: Score scatter plot of PC1 vs. PC 2. [t1] Scores of Principal Component 1; [t2] Scores of Principal Component 2.

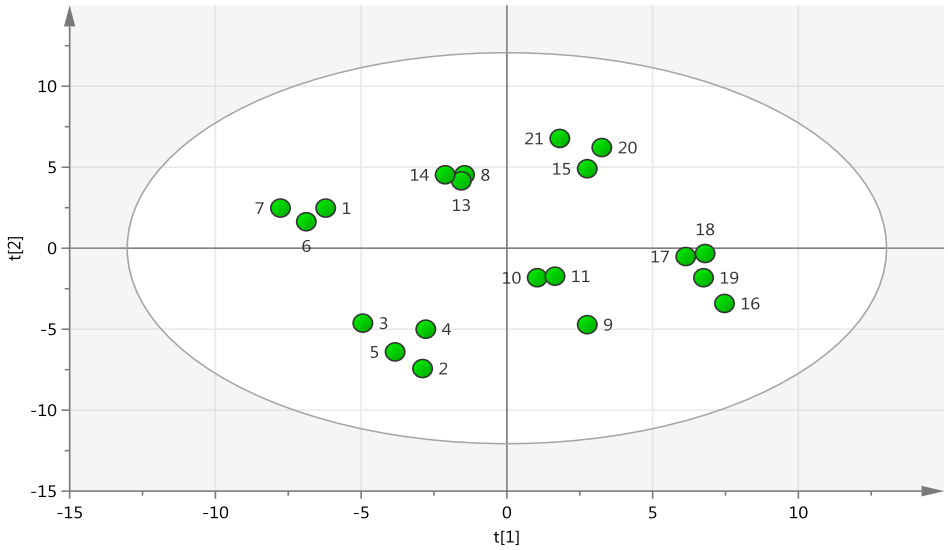

Figure 9: Loading scatter plot of PC1 vs. PC 2. [p1] Scores of Principal Component 1; [p2] Scores of Principal Component 2. Key: see Table 2 and Table 3.

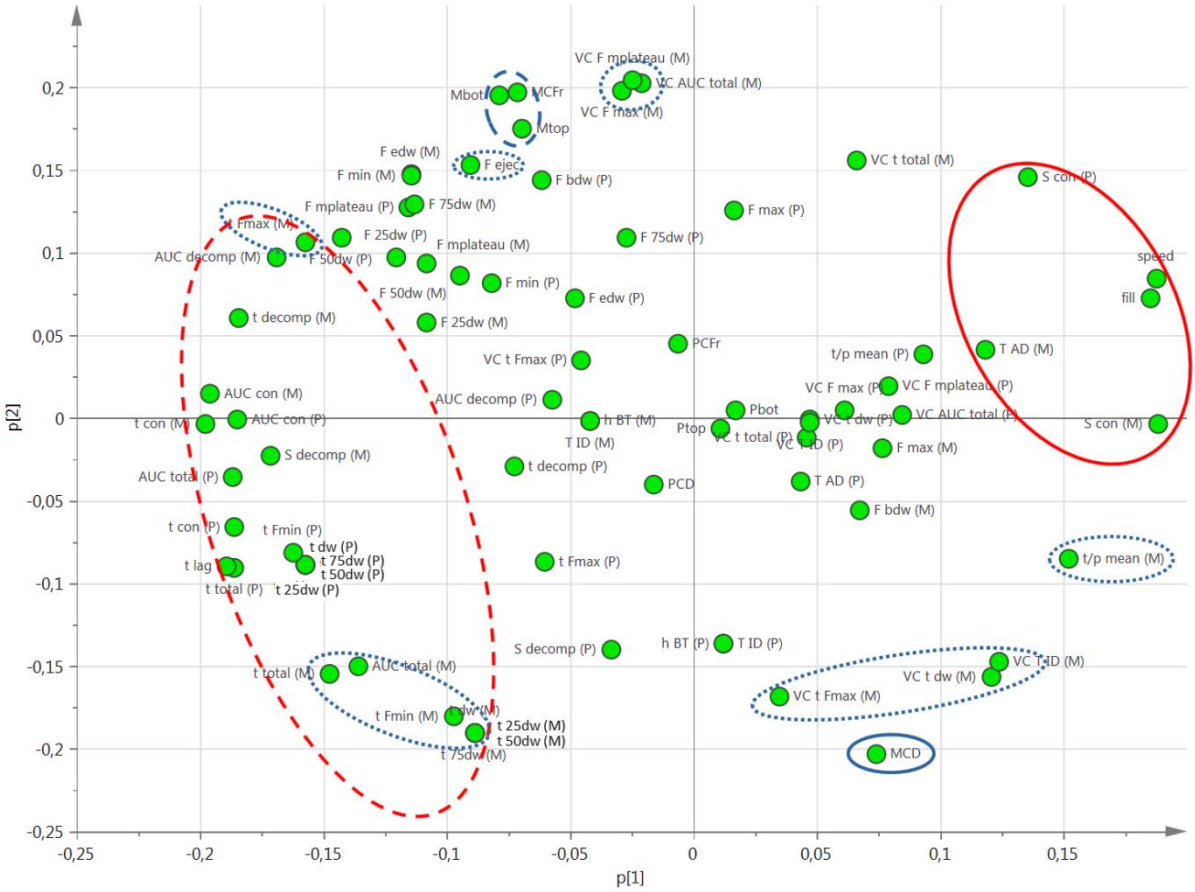

Figure 10: Score scatter plot of PC3 vs. PC 4. [t3] Scores of Principal Component 3; [t4] Scores of Principal Component 4.

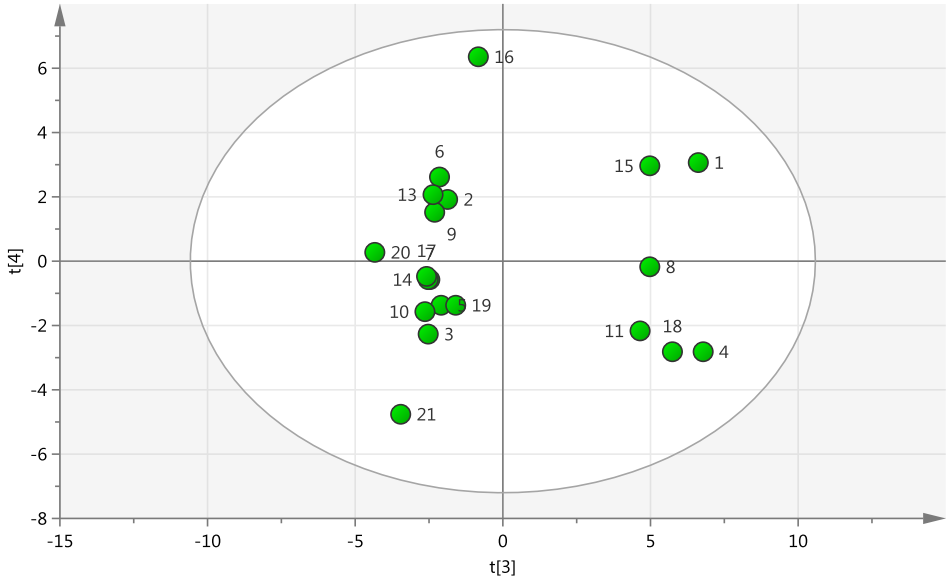

Figure 11: Loading scatter plot of PC3 vs. PC 4. [p3] Loadings of Principal Component 3; [p4] Loadings of Principal Component 4. Key: see Table 2 and Table 3.

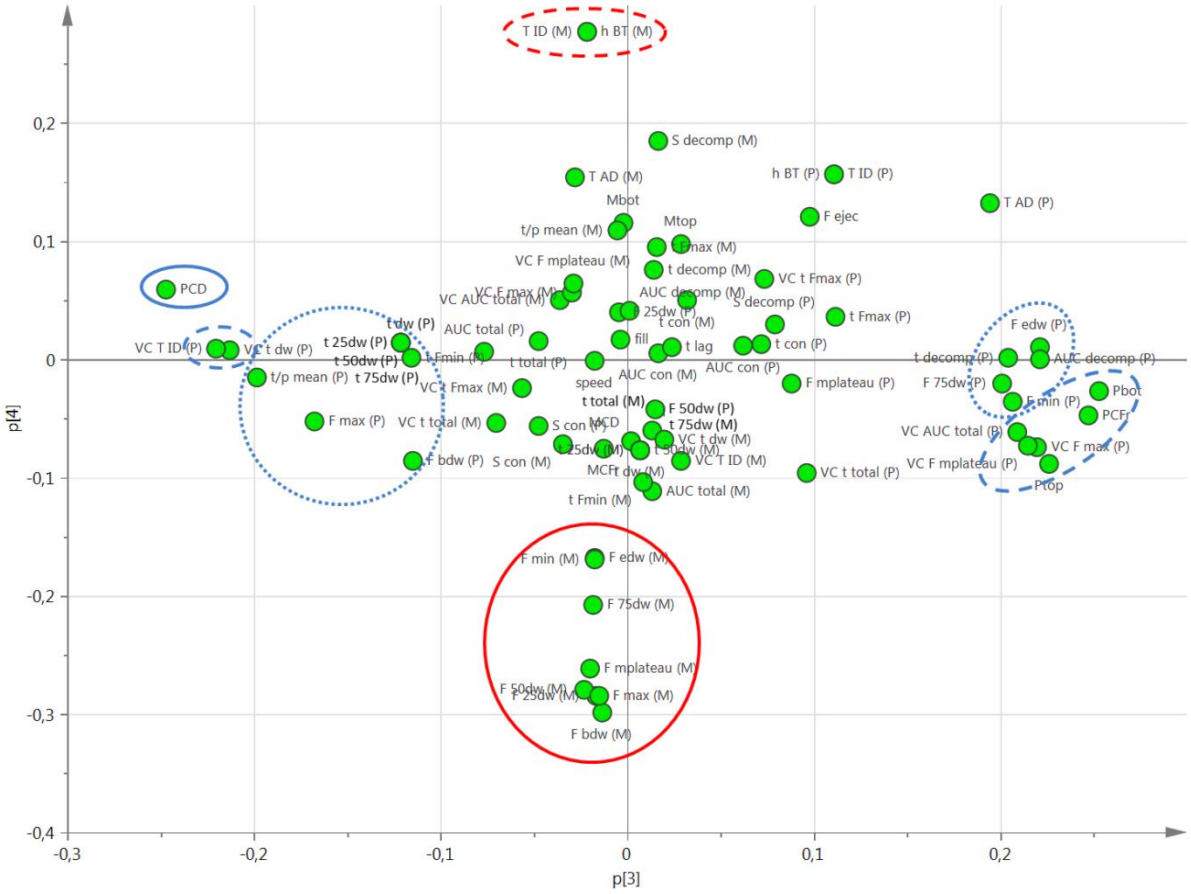

Figure 12: Score scatter plot of PC1 vs. PC 2. [t1] Scores of Principal Component 1; [t2] Scores of Principal Component 2.

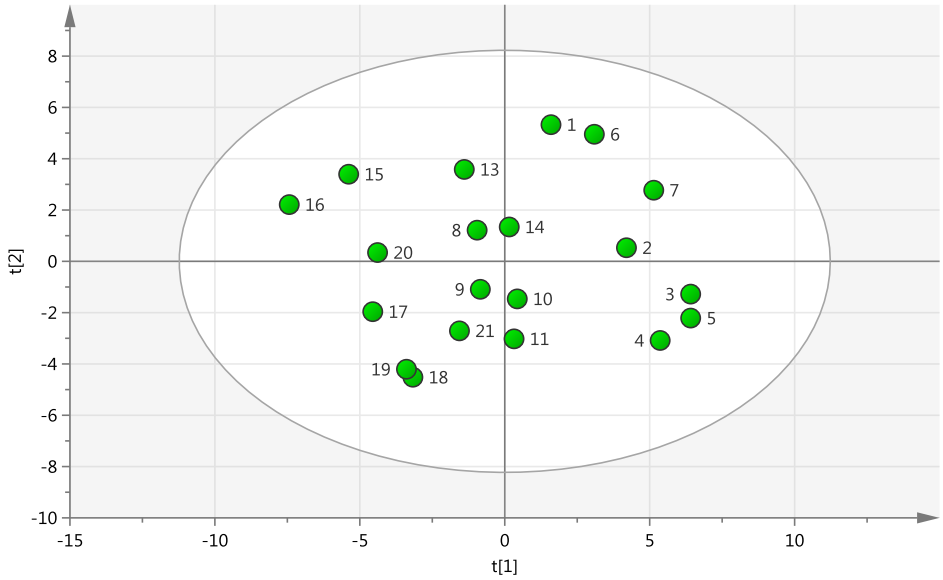

Figure 13: Loading scatter plot of PC1 vs. PC 2. w*c[1] Loadings of Principal Component 1; w*c[2] Loadings of Principal Component 2. Key: see Table 2, Table 3 and Table 4.

Figure 14: Score scatter plot of PC2 vs. PC 3. [t2] Scores of Principal Component 2; [t3] Scores of Principal Component 3.

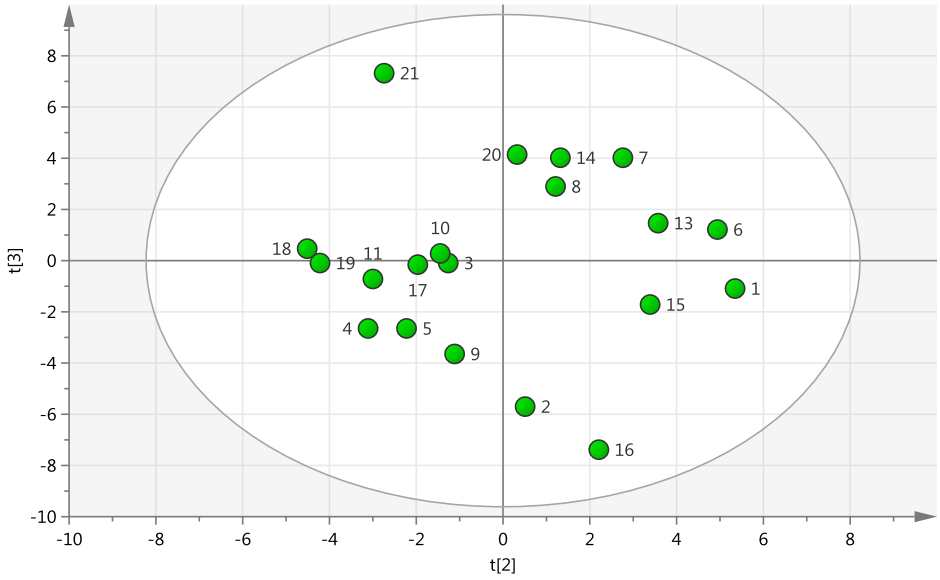

Figure 15: Loading scatter plot of PC2 vs. PC 3. w*c[2] Loadings of Principal Component 2; w*c[3] Loadings of Principal Component 3. Key: see Table 2, Table 3 and Table 4.